CHEMISTRY OF MATERIALS
Review

Chem. Mater. **2011,** *23,* 733–758 733
DOI:10.1021/cm102419z

π-Conjugated Polymers for Organic Electronics and Photovoltaic Cell Applications[†]

Antonio Facchetti*

Polyera Corporation, 8045 Lamon Avenue, Skokie, Illinois 60077, United States, and Department of Chemistry and the Materials Research Center, Northwestern University, 2145 Sheridan Road, Evanston, Illinois 60208-3113, United States

Received August 23, 2010. Revised Manuscript Received November 21, 2010

The optoelectronic properties of polymeric semiconductor materials can be utilized for the fabrication of organic electronic and photonic devices. When key structural requirements are met, these materials exhibit unique properties such as solution processability, large charge transporting capabilities, and/or broad optical absorption. In this review recent developments in the area of π-conjugated polymeric semiconductors for organic thin-film (or field-effect) transistors (OTFTs or OFETs) and bulk-heterojunction photovoltaic (or solar) cell (BHJ-OPV or OSC) applications are summarized and analyzed.

1. Introduction

The interest in π-conjugated polymers increased considerably after the discovery that their electrical conductivity increases substantially upon electrochemical doping.[1] This discovery led to the 2000 Nobel Prize in Chemistry awarded to Alan Heeger, Alan MacDiarmid, and Hideki Shirakawa. By the mid-1980s, several research teams in both academia and industry were investigating π-conjugated small molecules and polymers to gain benefit of their unique optical and semiconducting properties, paving the way to the emergence of the fields of plastic electronics and photonics.[2] These new technologies are thought to compliment current inorganic-based optoelectronic devices, which greatly impacted our society starting from the second half of the 20th century. The goal of organic-based opto-electronic devices is not that of attaining or exceeding the level of performance of silicon technologies but of enabling the fabrication of certain optoelectronic devices (or part of them) at far reduced costs and/or enabling completely new device functionalities (e.g., mechanical flexibility, impact resistance, and optical transparency) that are challenging to achieve with silicon.[3]

Besides the discovery of new materials, the development of organic semiconductor-based opto-electronics requires achieving a much better understanding of the nature of electronic structure and charge transport properties, as well as light-molecule/polymer and charge−charge interactions, in these unusual solids.[4] Although these aspects are fundamental for the optimization of these materials, the goal in this contribution is to review very recent achievements in the development of polymeric semiconductors for charge transport in thin-film transistors (TFTs) and energy production in bulk-heterojunction photovoltaic (PV) cells. Particularly we will first introduce basic concepts of organic polymeric semiconductor structure and OTFT/OPV operation and then focus exclusively on the works of the last three years since excellent OTFT[5] and OPV cell[6] review articles cover previous fundamental and evolutionary studies.

2. Polymeric Semiconductors

Polymeric semiconductors for OTFT and OPV applications must present two essential structural features (Figure 1).[7] The first is a π-conjugated backbone composed of linked unsaturated units resulting in extended π orbitals along the polymer chain, thus enabling proper charge transport and optical absorption.[8] The second is the functionalization of the polymer core with solubilizing substituents, which is essential for inexpensive manufacture by solution methods as well as to enhance solid state core interactions.[9] Among the most common unsaturated units there are mono(poly)cyclic aromatic hydrocarbons, heterocycles, benzofused systems, and simple olephinic and acetylinic groups. The extent of conjugation/interaction between these units determine the polymer solution/solid state electronic structure, which in turn control key polymer properties such as optical absorption/emission, redox characteristics, and frontier molecular orbital energy levels, to cite just a few properties.

Other important polymer architecture parameters are the molecular weight (M_w) and the polydispersity (PD) index since they influence solubility, solution aggregation, and formulation rheology, as well as the thin film formation and morphology for both pristine and blended materials. Since when going from low (oligomers) to high (polymer) molecular weights the electronic structure, thermal properties, and microstructure of polymers generally vary considerably, it is important to achieve a M_w/PD regime where certain a

[†] Accepted as part of the "Special Issue on π-Functional Materials".
*E-mail: afacchetti@polyera.com or a-facchetti@northwestern.edu.

Published on Web 12/23/2010

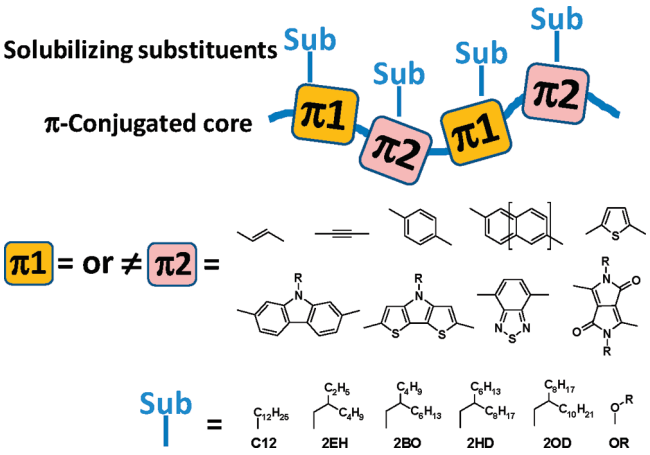

Figure 1. Schematic representation of a polymer chain showing very few examples of unsaturated (π) and solubilizing (sub) units.

property stabilizes, so that greater reproducibility of the polymer property from batch to batch can be achieved. This value is likely to be strongly dependent on the polymer structure; however, for most soluble thiophene-based polymers, a number average molecular weight value of about 20−30 kDa and a PD of 1.2−1.8 are reasonable for these threshold values.[10]

There are several advantages in using polymeric versus molecular π-conjugated semiconductors. Thin films of polymeric materials are generally very smooth and uniform, enabling a great control over large scale of the film structural and morphological characteristics. Printing requires great control of the solution rheological properties, which can be tuned efficiently for polymer-based solutions. Polymer crystalline domains are typically much smaller than the length scale of several opto-electronic devices resulting in isotropic transport characteristics. This results in low device-to-device performance variability, which is particularly important for TFT integration into circuits. Furthermore, fabrication of multilayers from solution deposition processes requires that each stacked layer is inert to the solvents and processing temperatures that it is subsequently exposed to during device manufacture. The reduced solubility parameter window of polymers, and their large bulk viscosity, typically increases the options to find orthogonal solvents for solution deposition on top of polymer layers, thus expanding the choice of materials that can be used in devices. Finally, since polymers do not vaporize before decomposition and thus have negligible vapor pressure, they are not susceptible to interlayer diffusion during the typical device-fabrication thermal cycles and typically exhibit robust mechanical properties, making nanometer-thick semiconductor films potentially compatible with roll-to-roll fabrication on flexible substrates.

3. Thin-Film Transistor Applications

Organic thin-film transistors are a low-cost technology alternative to amorphous hydrogenated silicon transistors for applications in large-area OTFT-based arrays, for example, backplane/driver circuits for active matrix

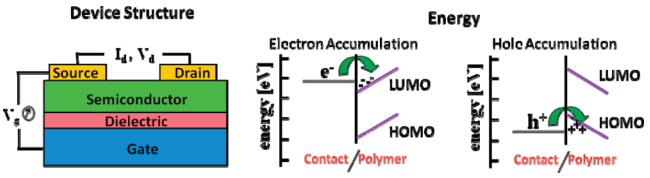

Figure 2. Structure and materials of bottom-gate top-contact thin-film transistors along with the energy levels of the contact-semiconductor materials where charge accumulation takes place.

displays, where high transistor density and switching speeds are not necessary. They may also be attractive for applications in low-end microelectronics (e.g., radio frequency identification tags, sensors, etc.) where the high cost of packaging conventional Si circuits is prohibitive for everyday items.[11] OTFT advantage stems from the potential lower manufacturing costs and reduced capital investments thanks to device fabrication using common solution-based deposition and patterning techniques such as offset, gravure, screen/stencil printing, and inkjet printing to cite just a few. Furthermore, OTFT-based circuits based on conjugated polymers are compatible with plastic substrates so that compact, lightweight, and structurally robust and flexible electronic devices can be fabricated.

Figure 2 shows a schematic structure of a bottom-gate top-contact OTFT. Note that several other device architectures can be fabricated depending on the relative position of the contacts and the dielectric/semiconductor layers (not shown). An OTFT is composed of three electrodes (source, drain, and gate), a gate dielectric layer, and an organic or polymer semiconductor layer. In this device, negligible source-drain current (I_{SD} = 0 A) flows when the gate voltage is zero (V_G = 0 V) independently of the bias applied between the source and the drain contacts (V_{SD}). The device turns ($I_{SD} \neq 0$ A) on when a gate field is applied ($V_G \neq 0$ V), which induces charge carrier in the semiconductor at the interface with the dielectric layer. The transistor performances are evaluated from the output and transfer current−voltage plots, where critical parameters such as the field-effect mobility (μ), current on/off ratio (I_{on}/I_{off}), threshold voltage (V_T), and subthreshold swing (S) are measured (Figure 3).

Within the metal oxide−semiconductor field-effect transistor gradual channel model approximation, the carrier mobility in the linear and in the saturation regimes can be extracted from the standard MOSFET equations:

$$(I_{SD})_{lin} = (W/L)\mu_{FET}C_i(V_{SG} - V_T - V_{SD}/2)V_{SD} \quad (1)$$

$$(I_{SD})_{sat} = (W/2L)\mu_{FET}C_i(V_{SG} - V_T)^2 \quad (2)$$

where V_{SD} is the drain voltage with the source electrode being grounded. W and L are the transistor channel width and length, respectively, and C_i is the capacitance per unit area of the dielectric layer. Polymeric semiconductors for TFTs can be divided into three classes depending if the majority charge carriers are holes (p-channel), electrons (n-channel), or both (ambipolar) under different gate bias

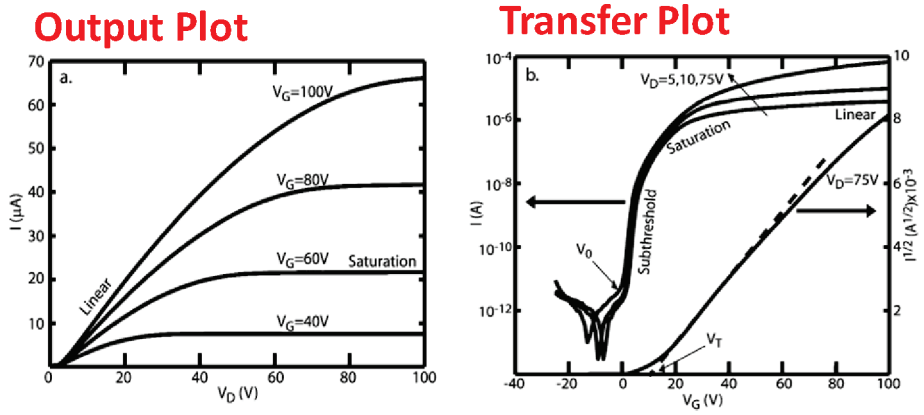

Figure 3. A. Output plot of the source−drain current versus the source−drain voltage at given V_G values. B. Transfer plot of the source−drain current versus the gate voltage at different V_{SD} values.

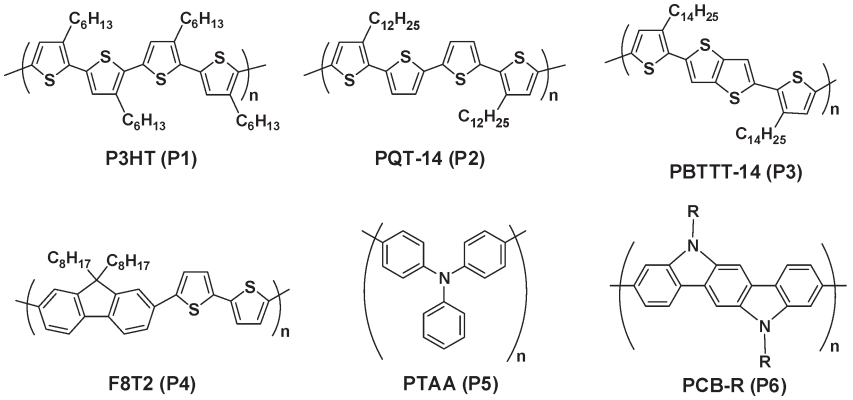

Figure 4. Chemical structure of the p-channel semiconductors **P1**−**P6**.

conditions. Until recently, polymeric semiconductors for TFTs were particularly challenging since most of them were difficult to synthesize/reproduce optimal batches, were poorly soluble, were very sensitive to ambient conditions, and/or exhibited poor charge carrier mobility. Insoluble polymers preclude their use with solution deposition techniques while air sensitivity requires manufacturing in cost-prohibitive inert atmosphere. However, during the last three years few polymeric semiconductors exhibit the combination of all required properties enabling the realization of OTFT meeting first-generation market products.

3.1. p-Channel Polymeric Semiconductors. To date, the majority of the satisfactorily performing polymers for OFETs are p-channel. Besides the basic structural requirements discussed previously, the common strategy to enable good hole-transporting polymers for TFTs is via a delicate balance of the HOMO energy level which should lie somewhere around $-5 \sim -5.5$ eV. When E_{HOMO} is too high (low ionization potential), facile oxidation by air and acceptor sites dramatically compromise TFT ambient stability and current on−off ratio. For $E_{HOMO} \ll -5.5$ eV (high ionization potential), very large I_{on}:I_{off} and good mobilities can be achieved; however, these devices typically suffer from unacceptably large threshold voltages.

In this section we will first summarize very briefly key historical p-channel polymers (Figure 4), considering their importance, and then discuss very recent developments. Poly(3-substituted thiophene)s (P3AT) are one of the most studied polymer families for (semi)conductor/optical applications.[12,13] These systems have the advantage that the presence of the 3-substituent strongly enhances solubility and processabilty. The performance of poly(3-alkylthiophene)-based OFETs, particularly P3HT (**P1**), have been investigated by various groups considering the effects of P3AT molecular weight,[14−16] film deposition solvent,[17] film morphology,[18,19] film thickness,[20] and fabrication process,[21] as well as humidity[22] and core substituent (alkyl chain) length.[23] These studies have deepened our understanding of the charge transport properties of polymeric semiconductors as a whole. However, it was challenging to achieve great control over regioregularity in several poly(3-alkylthiophene) syntheses, and exposure of P3AT films to air usually causes an increase in carrier density, thus degrading the transistor I_{on}:I_{off}. Therefore, high I_{on}:I_{off} for P3AT are consistently achieved in preparing and testing the devices in dry N_2.[24] To address these problems new polythiophenes have been developed. Ong et al. report a class of solution-processable regioregular polyquaterthiophenes (PQTs) that affords excellent FET performance under ambient conditions. This class of polythiophenes was designed on the basis of the following structural considerations: (i) Presence long alkyl sidechains for solution processability; (ii) structural regularity to induce and facilitate molecular self-assembly; and (iii) control of the conjugation extension to achieve a delicate

balance between transistor functionality and oxidative doping stability. These semiconductors exhibit unique self-assembly ability and form highly structured thin films when deposited from solution under appropriate conditions. FETs fabricated in air with PQT-12 (**P2**, Figure 4) channel layers have provided high field-effect mobility up to 0.14 $cm^2/(V\,s)$ and high $I_{on}:I_{off} > 10^7$.[25] Chabinyc et al. investigated the effects of humidity on unencapsulated **P2**-based OFETs. The field effect mobility of **P2** TFTs decreases and the rate of trapping of charge carriers increases under increasing humidity,[26] pointing out that not only n-channel semiconductors are H_2O-sensitive.

Rather than increase the ionization potential of polythiophene by sterically twisting the repeat units in the backbone, McCulloch et al. synthesized polymers incorporating thieno[3,2-*b*]thiophene (**P3**)[27,28] as comonomers. The delocalization of electrons from the fused aromatic units into the backbone is less favorable than from a single thiophene ring, due to the larger resonance stabilization energy of the fused ring over the single thiophene ring. The decreased delocalization along the backbone lowered the polymer highest occupied molecular orbital (HOMO) level. The charge-carrier mobilities of **P3** are high, with values of 0.2−0.6 $cm^2/(V\,s)$ obtained on annealed devices in a nitrogen atmosphere and up to 0.7 $cm^2/(V\,s)$ for 5 μm channel length devices. DeLongchamp et al. investigated in detail the origin of the enhanced crystallinity of this polymer.[29] From first-principles energy minimization using density functional theory, the authors predicted that the conjugated polymeric planes of **P3** are substantially tilted within their crystalline lamellae. This prediction was confirmed experimentally using a combination of polarized photon spectroscopies including NEXAFS and IR. Other important first-generation polymeric semiconductor families are those based on 9,9-dialkylfluorene-*alt*-triarylamine (e.g., TFB, **P4**),[30,31] triarylamine (**P5**),[32] and carbazole (e.g., PCB, **P6**)[33,34] units (Figure 4).

During the last three years, several new structures, particularly based on fused units, have been developed, resulting in even greater p-channel TFT performances (Figure 5). Rasmussen and co-workers pioneered the use of *N*-alkyldithieno[3,2-*b*:2′,3′-*d*]pyrrole (DTP) as a very promising fused aromatic building block for electronic materials.[35] This core exhibits a completely flat crystal structure, indicating good π conjugation across the fused rings. Upon polymerization, poly(*N*-alkyl dithieno[3,2-*b*:2′,3′-*d*]pyrrole)s exhibit excellent stability in their oxidized state, have low band gaps, and show efficient red fluorescence in solution.[36] However, some PDTPs have low solubilities and low molecular weights, which greatly limits their use in devices. To improve the solubility of PDTPs and to create a number of DTP-based copolymers, McCullough et al. described the synthesis, characterization, electrical conductivity, and field effect mobility of a series of novel soluble *N*-alkyl DTP−thiophene copolymers (**P7**−**P12**, Figure 5) and compared them to well-studied regioregular P3HT.[37] These polymers were synthesized using a Stille coupling reaction and exhibited molecular weights of 10−50 KDa. The incorporation of planar DTP

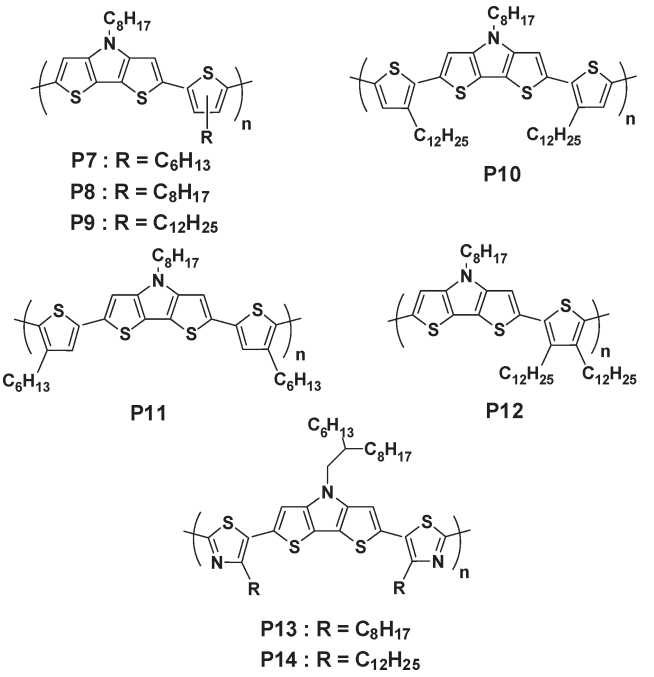

Figure 5. Chemical structure of dithienopyrrole-based p-channel semiconductors **P7**-**P14**.

units extends π conjugation, and the introduction of thiophene subunits imparts good solubility, high conductivity, and high charge carrier mobility. Optical characterization revealed that the band gaps of **P7**−**P12** were between 1.74 and 2.00 eV, lower than regioregular poly (3-alkylthiophenes), and the HOMO energy levels are between −4.68 and −4.96 eV. When doped, these polymers exhibited high conductivities up to 230 S/cm with excellent stability. The microstructure and surface morphologies of, for instance, poly(2-(4,4′-didodecyl-2,2′-bithiophen-5-yl)-4-octyl-4*H*-bisthieno[3,2-*b*:2′,3′-*d*]pyrrole) (**P10**) thin films were studied by X-ray diffraction and atomic force microscopy. As-cast **P10** thin films exhibited poorly defined, randomly ordered lamellar structure that improved significantly after thermal annealing (Figure 6). Field effect transistor devices showed typical p-channel transistor behavior. Interestingly, the mobilities of as-cast, less ordered samples were much higher than those observed after annealing. The highest values of maximum and average mobilities were observed for **P10** as-cast (0.21 and 0.13 $cm^2/(V\,s)$, respectively). The authors' goal was to test the idea that high mobility and excellent electrical and structural reproducibility could be achieved in amorphous π-conjugated materials that could possess long range π connectivity on the microscopic scale.

To improve air stability of these materials the authors have included electron deficient units into the polymer backbone to increase the ionization potential.[38] To this end, the same group has used the electron-deficient thiazole (Tz) unit, which is known to increase IP.[39] The new polymers **P13** and **P14** (Figure 5), defined as "transistor paints", achieved excellent FET performance with hole mobilities as high as 0.14 $cm^2/(V\,s)$ and 0.10 $cm^2/(V\,s)$, and current on/off ratios up to 10^6 without post-deposition thermal annealing. Furthermore, these devices exhibited excellent

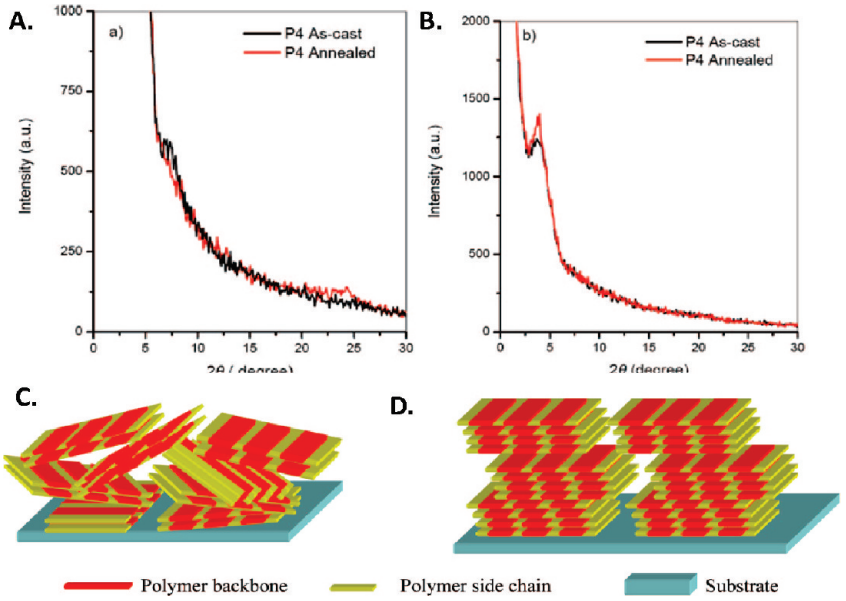

Figure 6. XRD profile of **P10** thin films on OTS-treated SiO_2/Si substrate as-cast (black trace) and after annealing at 120 °C for 30 min (red trace). (A) Out-of-plane XRD profile. (B) In-plane XRD profile. Scheme of molecular packing of **P10** (C) as-cast and (D) after annealing at 120 °C for 30 min. Adapted with permission from ref 37. Copyright 2008 American Chemical Society.

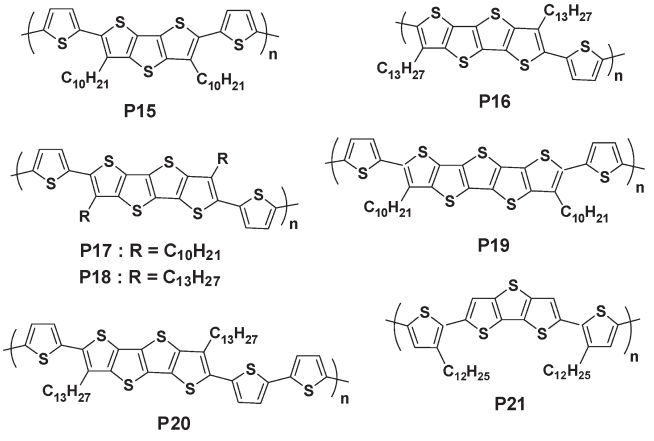

Figure 7. Chemical structure of fused thiophene-based p-channel semiconductors **P15**−**P21**.

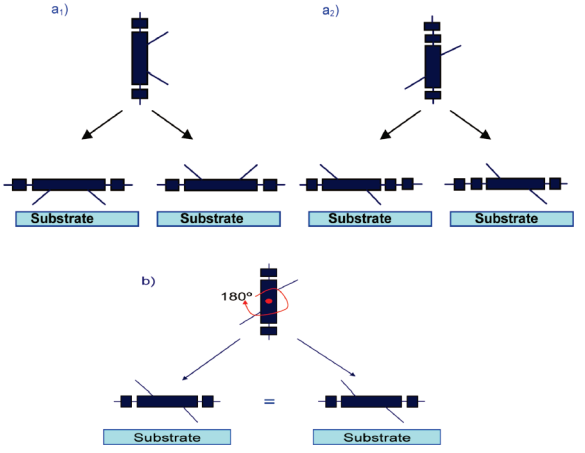

Figure 8. Possible configurations of the repeat unit with respect to the substrate, for repeat units (a1 and a2) without and (b) with *C*2 symmetry. Judging from the family of closely related conjugated polymers that we have investigated, *C*2 symmetry seems to enable a very small lamellar period and promote high mobility. Reprinted with permission from ref 41. Copyright 2010 American Chemical Society.

air stability, showing no significant degradation over 60 days.

He, Malliaras, and co-workers recently reported a family of fused-ring thiophene copolymers (**P15**−**P20**, Figure 7), as materials of interest for thin film transistor applications.[40] In an initial study, a comparison of the properties of **P15**−**P17** showed that the polymer with the even-numbered fused-thiophene core exhibits a much smaller lamellar spacing than the polymers featuring odd-numbered fused-thiophene cores. As a result, transistors fabricated from polymer with the even-numbered fused-thiophene core (**P16**) yielded a much higher field-effect mobility than the other two (**P15** and **P17**). To obtain further insights into the structure−property relationships in these polymeric semiconductors, more recently they included additional polymers which were used to elucidate the role of symmetry of the polymer repeat unit on structure and device performance (Figure 8). Devices made from the polymer with the four fused rings (**P17**) showed a hole mobility of 0.087 $cm^2/(V\ s)$, whereas devices made from the polymers with the three fused rings (**P15**) and five fused rings (**P17**) showed hole mobilities of 0.0017 and 0.0023 $cm^2/(V\ s)$, respectively. Devices made from **P16** and **P20** showed a hole mobility of 0.042 and 0.022 $cm^2/(V\ s)$, respectively, which is ∼10× lower than 0.33 $cm^2/(V\ s)$ achieved with **P18**.[41] These results strongly suggest a correlation between a repeat unit that possesses a C2-axis perpendicular to the conjugation plane, a minimum attainable lamellar spacing, and a high field-effect mobility. Interestingly, Ong and co-workers reported a new dithienothiophene-based copolymer, **P21**, as structurally similar polymers as **P15**, and showed mobilities of ∼0.01 $cm^2/(V\ s)$,[42] corroborating these symmetry-driven trends.

Muellen et al. developed benzo[2,1-*b*;3,4-*b*0]dithiophene-containing homo- and copolymers (**P23**−**P26**, Figure 9) having solubilizing alkyl chains attached to the benzo unit[43] alternatives to the classic TBT-based copolymer

P22.[44] The homopolymer **P23** is very soluble in dichlorobenzene, and top-contact TFTs exhibit low charge-carrier mobility of $\sim 10^{-4}$ $cm^2/(V\ s)$, probably because the polymer backbone is too stiff. The other copolymers exhibit greater performance ranging from 0.001 to >0.1 $cm^2/(V\ s)$ for bottom-gate top-contact transistors. Top-gate devices based on **P26** on a polyethylene terephthalate (PET) film were also fabricated and exhibit exceptionally large carrier mobility >0.5 $cm^2/(V\ s)$.

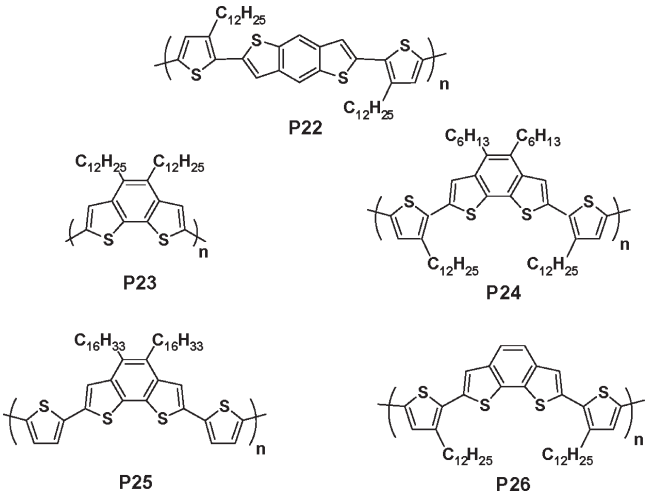

Figure 9. Chemical structure of fused thiophene-based p-channel semiconductors **P22**−**P26**.

Among the approaches to increasing air stability, the incorporation of unsubstituted conjugated moieties in poly(alkylthiophene) backbones resulted in much better oxidative stability and hole mobility, as demonstrated in PQT (**P2**) and pBTTT (**P3**). These unsubstituted conjugated moieties possess rotational freedom, which reduces the effective conjugation length, lowers the HOMO level, and consequently increases oxidative stability. Unsubstituted thiophene moieties, along with lengthened alkyl side chains, play also another important role by promoting favorable interdigitation of the side chains. This leads to well-organized intermolecular 3D ordering and large crystalline domains, and consequently high mobility. Thienylenevinylene derivatives, a combination of thiophene and vinyl groups, are known to have an extended conjugated system, which is a crucial component for building organic electronic devices.[45] In addition, incorporating vinylene bonds in an aromatic polymer backbone leads to an increase of the degree of coplanarity of the polymer backbone, as the vinylene bond reduces steric hindrance of nearby aromatic rings.[46] Recently Kim et al. reported high-performance OTFTs with a new thienylenevinylene polymer **P27** (Figure 10). An unsubtituted dithienylethylene unit is symmetrically inserted in between the dodecylthiophenes, which enhances core rotational freedom and thus lowers the HOMO level. **P27**-based OTFTs showed unoptimized charge-carrier

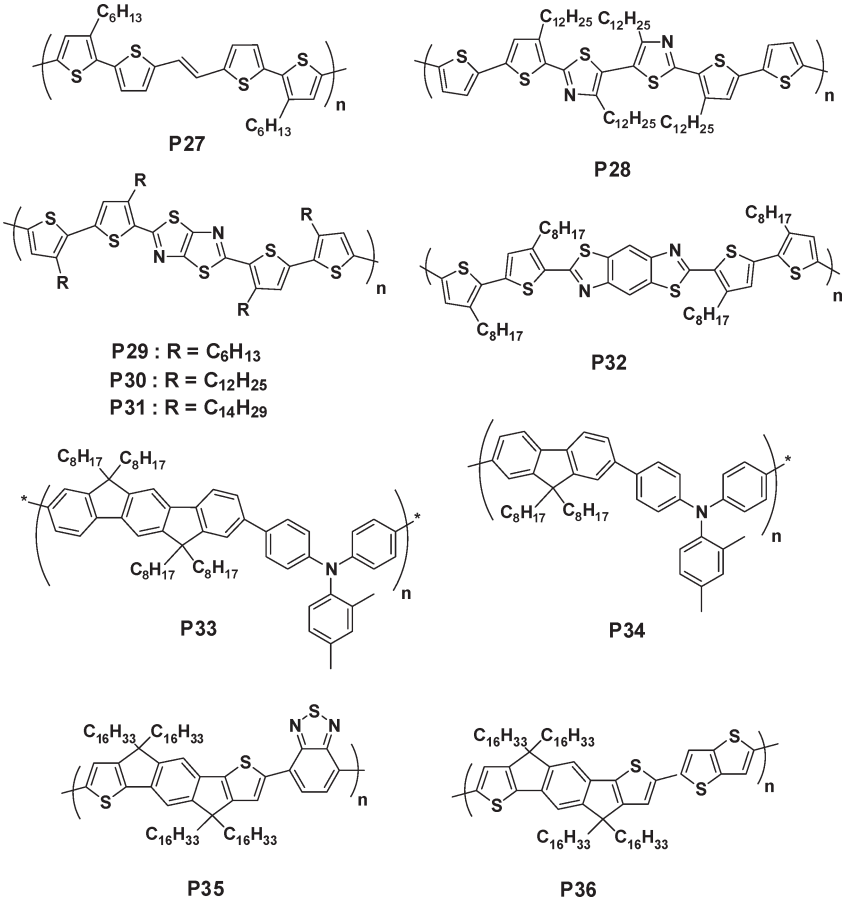

Figure 10. Chemical structure of p-channel semiconductors **P27**−**P36**.

mobility of 0.15 $cm^2/(V\ s)$ with a relatively high oxidative stability.

Some interesting structures incorporating the thiazole ring have been reported, mainly with the goal to increase oxidative stability. Another common problem with OFETs is the electrical instability under external bias stress, likely due to charge traps created through partial disorder in the structure of the thin films and the chemical characteristics of the semiconductor/insulator interface. Bias-stress instability and environmental instability can be significant challenges for semiconducting polymers.[47] To be usable in conventional electronics, OTFTs should exhibit similar characteristics with respect to electrical bias stress.[48] Although there have been a few studies aimed at enhancing the electrical stability of π-conjugated polymers under external bias stress, an adequate understanding of the relationship between crystalline nanostructure and bias stress driven electrical instability on the microscopic scale is still needed. Lee and co-workers have initiated an in-depth and systematic study addressing bias stress in polymers using highly ordered π-conjugated copolymer thin films with minimal concentration of charge traps.[49] They used a new thiazole polymer, **P28** (Figure 10), having alkyl chain-substituted thiophene/thiazole blocks along the polymer backbone to increase the IP because of the enhanced rotational freedom along the backbone[50] and the electron-accepting nature of the 5,5′-bithiazole units.[51] In particular, **P28** presents a liquid-crystalline nature with a clear mesophase region, resulting in highly crystalline thin films forming spontaneously through the self-assembly of individual chains after thermal annealing (Figure 11). Most important, this novel polymer exhibits high field-effect mobilities of 0.33 $cm^2/(V\ s)$, good environmental stability, and unprecedented bias-stress stability comparable to that of amorphous silicon.

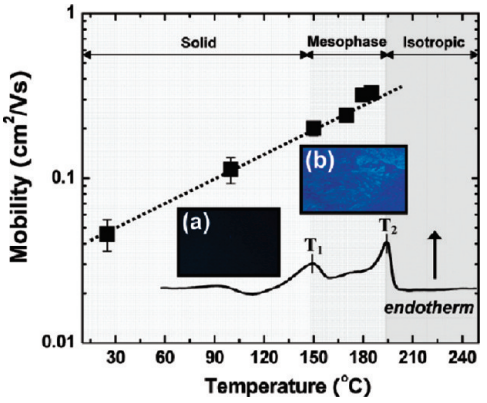

Figure 11. Variation in the charge-carrier mobility in **P28**-based OTFTs for films annealed at different temperatures. The inset shows the DSC curve, representing the liquid-crystalline mesophase and POM images of the samples annealed at (a) 100 °C and (b) 180 °C, respectively. Reprinted with permission from ref 49. Copyright 2009 American Chemical Society.

McCullough et al. reported copolymers (**P29**−**P31**) incorporating a fused thiazolothiazole ring in the backbone.[52] Despite the low molecular weights of this family (M_n = 4−9 KDa) they exhibit field-effect mobilities from 0.02 to 0.3 $cm^2/(V\ s)$ with high current on/off ratios of $\sim 10^6$. The use of the thiazolothiazole-fused ring ensures a very rigid and coplanar backbone and thereby highly extended π-electron conjugation and strong π stacking. The electron-deficient nature of the thiazolothiazole affords high oxidative stability. However, the uneven placement of the alkyl side chains along the backbone reduced interdigitation and promoted amorphous-like π-stacking and π-connectivity along the chain while enhancing solubility. In regard to side chain arrangement, the key difference between the **P29**−**P31** family and PBTTT/PQT polymers is that while the side chains in these polymers are still arranged regiosymmetrically, they are not equally spaced along the backbone. Thus, as a consequence, the side chains are apparently disordered and do not interdigitate as seen in PBTTT or PQT (Figure 12). Most interestingly, despite all these factors, X-ray diffraction

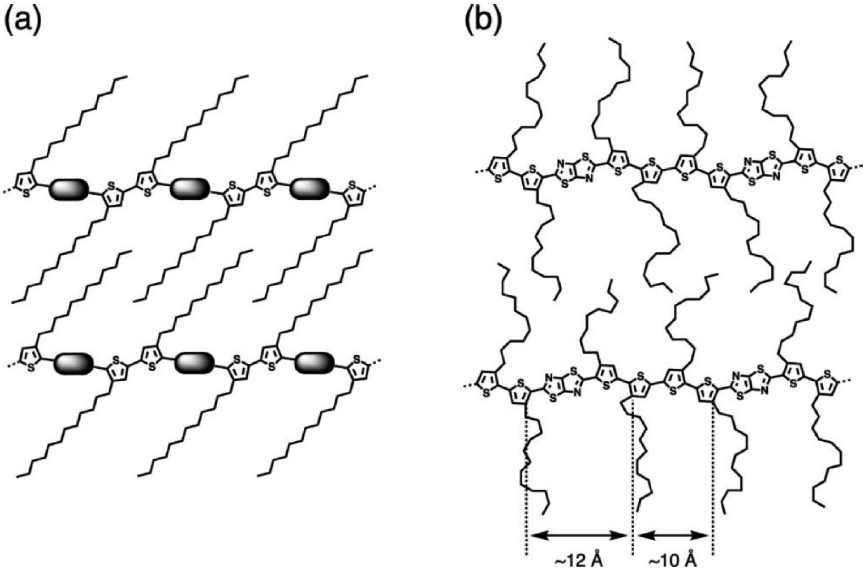

Figure 12. Schematic illustrations for (a) the packing structure of PQT (**P2**) and PBTTT (**P3**) with dodecyl side chain with uniform side chain interdigitation and (b) proposed packing structure for **P30** with disordered side chains. Reprinted with permission from ref 52. Copyright 2009 American Chemical Society.

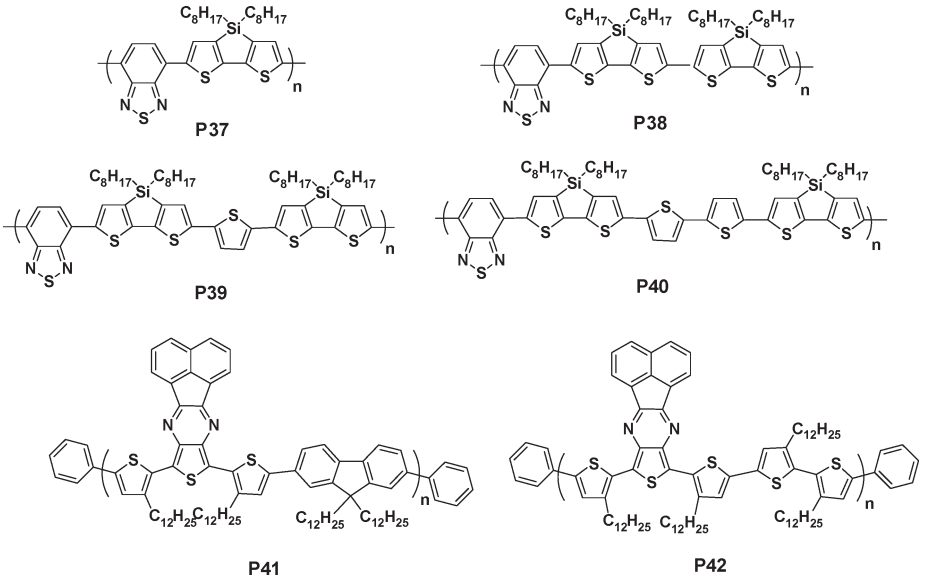

Figure 13. Chemical structure of p-channel semiconductors **P37**−**P42**.

patterns of **P29** indicate very strong lamellar ordering, and field-effect transistors fabricated from these materials show high-field-effect mobilities. All these results appear quite surprising in view of earlier mentioned findings on the role of side chain interdigitation/ordering and indicate that the strong interdigitation and formation of extended regular terracelike structures is not necessary for high carrier mobility in polythiophene-like materials.

Jenekhe and co-workers reported an interesting polymer, **P32** (Figure 10), designed with the knowledge that benzobisthiazole and benzobisoxazole polymers and small molecules exhibit efficient π-stacking and strong intermolecular interactions in the solid state[53] leading to high-temperature resistance with glass transition temperatures that can exceed 300−400 °C and relatively high electron affinity.[54] Earlier studies of a benzobisthiazole polymer as an n-channel semiconductor in field-effect transistors observed a low mobility of electrons, requiring a high electron affinity polymer in a blend to achieve electron injection.[55] Recently, thin film transistors based on benzobisthiazole small molecules exhibit high field-effect mobilities for both holes and electrons (vide infra).[56] The authors reported new soluble benzobisthiazole−thiophene copolymer based on alternating benzobisthiazole and oligo-3-octylthiophene units in the backbone (**P32**) having improved oxidative stability, thermal stability, and interchain interactions, thus enhancing the charge transport properties of the polymers. The highly crystalline **P32** thin films exhibit a field-effect carrier mobility of up to 0.01 $cm^2/(V\ s)$.

In two recent communications, Zhang and co-workers reported two classes of polymers based on fluorene and indenofluorene copolymerized with triarylamine (**P33** and **P34**)[57] and indacenodithiophene copolymerized with benzothiadiazole and thienothiophene (**P35** and **P36**).[58] Bottom-contact, top-gate (and bottom-gate) architecture field effect transistor devices based on **P33** and **P34** were fabricated with the polymer semiconductors deposited from solution. Compared to the best triarylamine homopolymers[59] (mobility of $\sim 4 \times 10^{-3}$ $cm^2/(V\ s)$), the new polymers exhibit improved mobility by a factor of 5 to 0.02 $cm^2/(V\ s)$ by the introduction of the fluorene unit and further increased to 0.04 $cm^2/(V\ s)$ for the indenofluorene copolymer and current on/off ratios $> 10^6$. It is speculated that the increase in polymer backbone planarity and persistence length in the copolymers improved the intramolecular π-orbital overlap as well as enhanced the local structural organization, resulting in the large measured mobilities. No evidence of thin film crystallinity could be observed for **P33** and **P34** polymer semiconductors. For polymers **P35** and **P36** the strategy for further improvement in charge carrier mobility in comparison to **P33** and **P34** was to enhance the planarity of the backbone and further reduce the energetic disorder of the polymer. The aryl amine unit was replaced with more planar BT and TT units. Grazing incidence X-ray scattering (GIXS) experiments were carried out on annealed thin films of both polymers on Si substrates to explore the microstructure, and **P35** polymer was observed to be semicrystalline while **P36** thin film was amorphous. Bottom-contact, top-gate (BC-TG) architecture field-effect transistor (FET) devices were fabricated with the polymer semiconductors spin-cast from a 10 mg/mL chlorobenzene solution at 2000 rpm followed by an annealing step at 100 °C for 5 min in nitrogen. **P35** transistors yield maximum hole mobilities in the range 0.8−1.2 $cm^2/(V\ s)$, with a current on/off ratio of $\sim 10^4$ and a threshold voltage of ~−30 V. Despite the very high mobility values, FET operation is heavily injection limited. The **P36** copolymer exhibits a lower mobility (~0.2 $cm^2/(V\ s)$), which is attributed to the more amorphous nature of the thin-film microstructure.

Inspired by work from Marks et al. on silole-based copolymers for TFTs,[60] Reynolds reported copolymers of dithienosilole with BTD, following the donor−acceptor concept to broaden the optical absorption (Figure 13).[61] DTS-BTD copolymers **P37**−**P40** differing by the

concentration of electron-donating and -withdrawing substituents along the backbone were synthesized and characterized by 2D-WAXS and in bottom-contact TFTs. While all copolymers self-assembled into lamellar morphologies, only **P38** and **P40** showed a propensity to π-stack. The highest hole mobility of 0.02 $cm^2/(V\ s)$ was observed for **P40** in agreement with the close π-stacking and lamellar distances found by structural analysis (0.36 and 1.84 nm, respectively). Following a similar strategy but by using different building blocks, Bao and co-workers synthesized dithiophene and fluorene copolymers (**P41** and **P42**) containing fused aromatic thieno[3,4-*b*]pyrazine moieties.[62] Suzuki and Stille polycondensation reactions were used for the polymerization. The band gap (E_g) of the polymers was tuned in the range of 1.15−1.6 eV. These polymers showed field effect mobility as high as 0.2 $cm^2/(V\ s)$ with current on/off ratios as high as 10^6 in OTFT devices.

Takimiya and co-workers reported several advanced molecular and polymeric semiconductors for TFTs with heteroarenes (Figure 14). The design rationale is that fusion of thiophene rings is necessary to avoid twisting between the adjacent thiophene rings, which would reduce the π stacking. A preliminarily synthesized benzothienobenzothiophene (BTBT)−thiophene copolymer (PBTBT, **P43**) resulted in a highly twisted backbone (λ_{max} < 400 nm), and TFTs based on this polymer did not function despite the fact that BTBT has been successful in small-molecule systems.[63] Thus this group recently presented a new design strategy based on **P44**−**P46** that incorporated naphthodithiophene (NDT) into a regiosymmetric polythiophene system.[64,65] These polymers showed high M_n of 24−33 KDa and sufficient solubility in warm chlorinated solvents. Thin-film transistors based on **P44**−**P46** exhibited among the highest field-effect mobility values observed to date for semiconducting polymers (> 0.3−0.5 $cm^2/(V\ s)$).

Finally, two additional interesting structures to report on are **P47** and **P48**. The first, developed by Wudl et al., consists of an electron donor (thiophene) and acceptor (cyclopentadienone) alternating copolymer (**P47**).[66] The results illustrate that despite the low molecular weight of this polymer (~6 KDa) a substantial field-effect mobility (~0.02 $cm^2/(V\ s)$) is obtained. The second, developed by Watson et al., is a copolymer of phthalimide and 3,3′-dialkoxy-2,2′-bithiophene (**P48**).[67] In this polymer backbone planarity is enforced by attractive intramolecular interactions between the pendant oxygens and thienyl sulfur atoms,[68] as shown by the crystal structures of some building blocks, intermolecular donor−acceptor interactions, and possibly increased quinoidal backbone character due to alternating donor and acceptor units.[69] The maximum field-effect mobilities were ~0.28 $cm^2/(V\ s)$ saturation region and current on/off current ratios of ~10^4−10^5 (Figure 15).

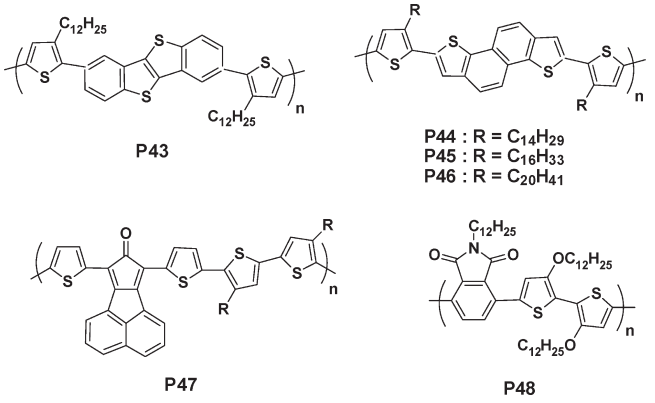

Figure 14. Chemical structure of p-channel semiconductors **P43**−**P48**.

3.2. N-Channel Polymeric Semiconductors. N-channel polymers for TFTs and, likewise, n-channel molecular systems have been traditionally underdeveloped compared to p-channel semiconductors. The reason for this deficiency in materials development was surprising considering that several experimental and theoretical studies suggested that organic semiconductors should transport electrons as or even more efficiently than holes. More recently, our understanding on how to enable efficient electron transport in TFTs increased after discovering the key role of other factors, besides the semiconductor electronic structure, affecting electron transport. These include: (1) Gate dielectric surface chemistry. Most of the first-generation dielectric materials for TFTs were oxides, such as SiOx, whose surfaces efficiently trap electrons. (2) Metal contacts.[70] Au has been traditionally used as source/drain TFT metal electrode. However, this results in a large energy barrier for electron injection. Thus, from an energetic perspective, low work function metals such

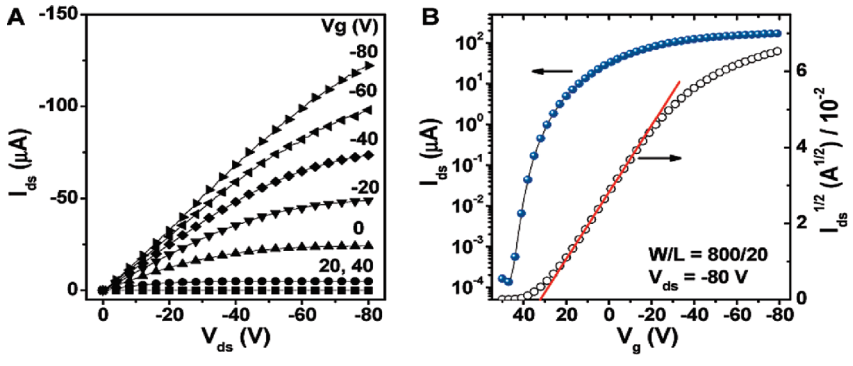

Figure 15. (A) Output and (B) transfer characteristics of **P48** thin-film transistor under ambient conditions. Reprinted with permission from ref 67. Copyright 2009 American Chemical Society.

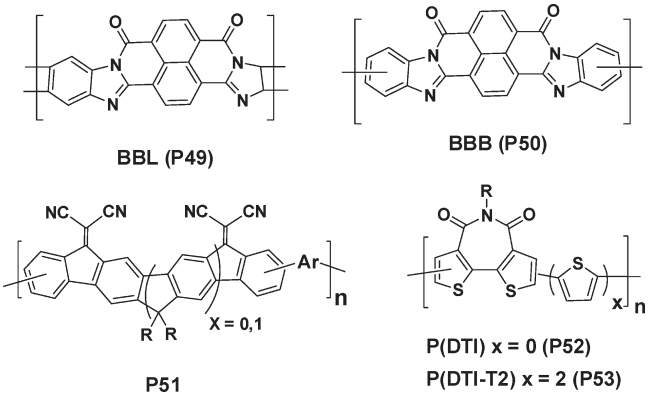

Figure 16. Chemical structure of n-channel semiconductors **P49**−**P53**.

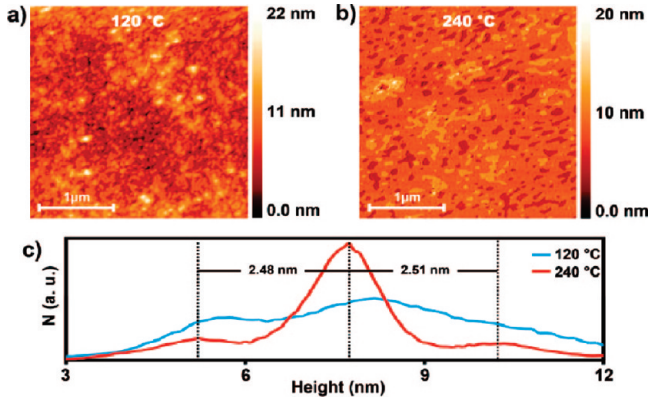

Figure 17. AFM images of **P52** films spin-cast from TCB and annealed at 120 °C for 30 min (a) and 240 °C for 2 h (b) and a height histogram (c) for both images (120 °C in blue and 240 °C in red) revealing formation of a terraced surface having a 2.50 nm step height. Reprinted with permission from ref 74. Copyright 2009 American Chemical Society.

as Al or Ca should be preferable. However, air-induced oxidation of these conductor surfaces result in an insulating layer, with the effect to vanish the benefit of having a formal lower energy barrier. (3) Ambient atmosphere composition. At the begin of the TFT field very few research groups carrying out materials development had the capabilities to perform measurements in inert atmosphere or vacuum. It is known that O_2 and H_2O can efficiently inhibit electron transport preventing several semiconductor classes to be screened for n-channel transport.

Today several of these issues can be controlled, and particularly the use of dielectric surface passivation strategies and polymeric dielectric materials have resulted in impressive progress in performance. From an energetic perspective, it is now believed that a quite narrow energetic window for the LUMO level, located at about $-4.0 \sim -4.3$ eV, must be achieved to enable polymeric semiconductors with good charge transport in ambient. For higher LUMO energy (low electron affinity), the polymer performance rapidly degrades after exposure to ambient atmosphere also when using electron-trap free dielectrics. On the other hand, for very low-lying LUMO systems (this has been well-established for molecular semiconductors), the corresponding devices are very difficult to turn-off.

In this section, we will describe a few first-generation n-channel polymers followed by more recent developments. The first report of an n-channel TFT-active polymer was poly(benzobisimidazobenzophenanthroline) (BBL, **P49**) and the corresponding BBB (**P50**) (Figure 16). This ladder-type polymer exhibits high electron mobility of 0.1 $cm^2/(V\ s)$ as spin-coated polycrystalline film[71] and ~0.01 $cm^2/(V\ s)$ for nanobelts.[72] In a series of papers the Northwestern group reported polymers based on the indenofluorene and bisindenofluorene core having C═O and C═C(CN)$_2$ substituents (**P51** family).[73] A novel design approach was employed using computational modeling to identify favorable monomer properties such as core planarity, solubilizing substituent tailorability, and appropriate electron affinity with gratifying results. Monomeric model compounds were also synthesized to confirm these properties, and crystal structures of several cores revealed short (<3.5 Å) $\pi-\pi$ stacking distance with favorable solubilizing substituent orientations. A family of 10 homopolymers and bithiophene **P51** copolymers was synthesized via Yamamoto and Stille polymerizations which exhibit n-channel mobilities approaching 10^{-3} $cm^2/(V\ s)$ in inert conditions.

The Northwestern group has also designed new homopolymers and copolymers based on the dithenodiimide core (**P52** and **P53**).[74] Two of these polymers are processable in common organic solvents: the homopolymer poly(*N*-(2-octyldodecyl)-2,2′-bithiophene-3,3′-dicarboximide) [P(DTI), **P52**] exhibits n-channel FET activity, and the copolymer poly(*N*-(2-octyldodecyl)-2,2′:5′,2″:5″,2‴-quaterthiophene-3,3′-dicarboximide) [P(DTI-T2), **P53**]) exhibits air-stable p-channel FET operation. After annealing, **P52** films exhibit a very high degree of crystallinity and an electron mobility > 0.01 $cm^2/(V\ s)$ with a current on−off ratio of 10^7, which is remarkably independent of film-deposition conditions. Extraordinarily, P(DTI) films also exhibit terracing in AFM images with a step height matching the X-ray diffraction *d* spacing, a rare phenomenon for polymeric organic semiconductors (Figure 17) .

Relevant n-channel polymers are those based on rylene dicarboxiimide cores, particularly perylene and naphthalene (Figure 18). The first perylene-based polymer [P(PDI2DD-DTT), **P54**] was synthesized by Stille coupling of *N*,*N*′-dialkyl-1,7-dibromo-3,4,9,10-perylene diimide with a distannyl derivative of dithienothiophene.[75] The M_w of P(PDI2DD-DTT) was not very high (~15 kD using GPC), and it was soluble in several solvents and could readily be processed from solution. DSC showed a glass-transition temperature of 215 °C, while TGA suggested excellent thermal stability with an onset decomposition temperature under nitrogen of 410 °C. Polymer **P54**-based OFETs (Al source/drain electrodes, top-contact/bottom-gate geometry) were measured under nitrogen and exhibit electron mobilities as high as ~0.01 $cm^2/(V\ s)$ and $I_{on}:I_{off} > 10^4$. Very recently, a dithienopyrrole analgue, **P55**, was reported to show an electron mobility of 7.4×10^{-4} $cm^2/(V\ s)$, which increases to 1.2×10^{-3} $cm^2/(V\ s)$ on annealing at 100 °C for 60 min under inert atmosphere.[76] The lower mobility observed for **P55** may be related to dilution of the electron-transporting unit by

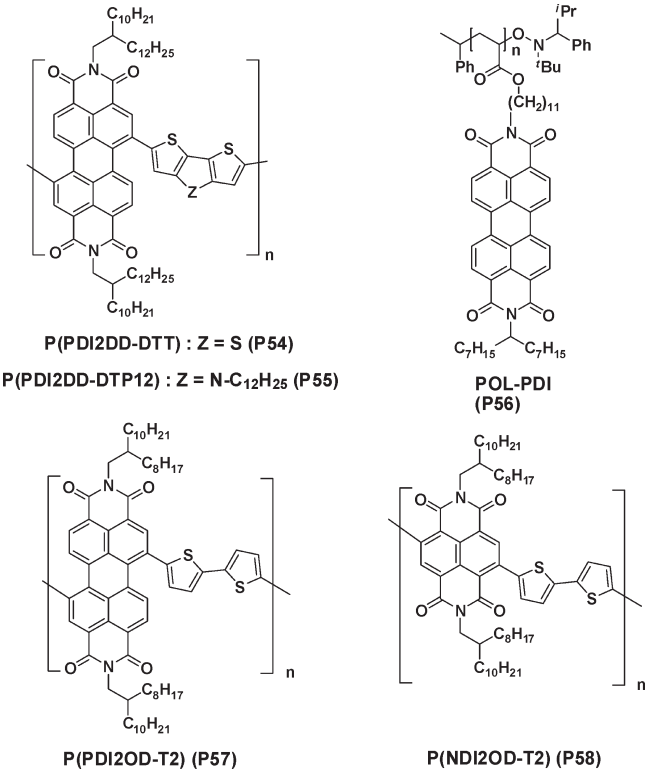

Figure 18. Chemical structure of n-channel semiconductors **P54**−**P58**.

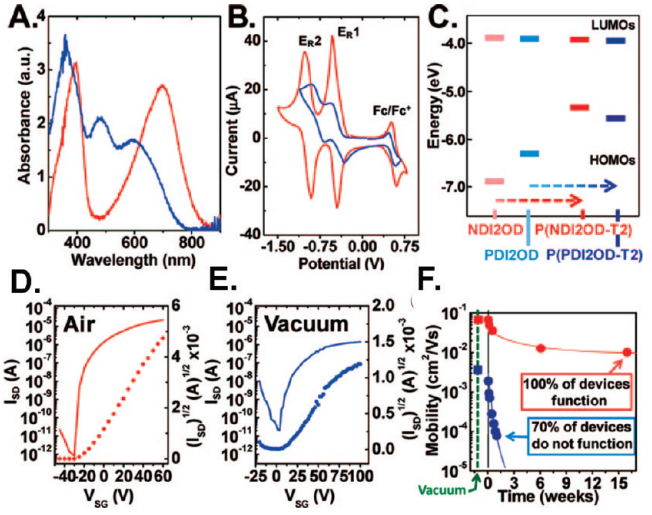

Figure 19. (A) Optical absorption spectra of spin-coated P(NDI2OD-T2) (red line) and P(PDI2OD-T2) (blue line) films (~30 nm thick) on glass. (B) Thin-film cyclic voltammetries [Fc (+0.54 V vs SCE) internal standard)] of P(NDI2OD-T2) (red line) and P(PDI2OD-T2) (blue line) thin films on a Pt electrode. The ER1 values of NDI2OD and PDI2OD (not shown) are −0.49 and 0.46 V vs SCE, respectively. (C) Energy diagram for the specified rylene monomers and polymers. (D) $I-V$ transfer plots for P(NDI2OD-T2) TFT in air for 1 h and (E) P(PDI2OD-T2) TFT in vacuum. (F) Polymer TFT electron mobility plots in vacuum and ambient (RH) 20−40%, $T \approx 25$ °C) vs time. Adapted with permission from ref 78. Copyright 2009 American Chemical Society.

the presence of the additional *N*-substituents of the dithienopyrrole donors. Thelakkat et al. have reported OFETs based on polymers containing the perylene unit as pendant groups such as **P56**.[77] For this polymer after thermal annealing at 210 °C for 60 min, the threshold voltage drops significantly to 7 V, while the current and charge carrier mobility both increase by 100× approaching to 1.2×10^{-3} cm^2/(V s). Unfortunately, OFETs based on these polymers are unstable in ambient conditions.

In recent works, the Polyera Corporation team reported the synthesis, characterization, and comparative properties of *N*,*N*′-dialkylperylenedicarboximide-dithiophene (PDIR-T2, **P57**) and *N*,*N*′-dialkylnaphthalenedicarboximide-dithiophene (NDIR-T2, **P58**) copolymers and the fabrication of the corresponding bottom-gate TFTs on Si-SiO_2 substrates.[78] The results of that paper demonstrate that the choice of the NDIR vs PDIR comonomer is strategic to achieve both high-performance bottom-gate n-channel TFTs and device functioning in ambient conditions. The rylene building block and the polymer structural design rationale were the following. (i) The electron-poor NDIR comonomer was selected because of the large electron affinity of this core, comparable to that of the far more π-extended PDIR systems. (ii) Equally important, NDIR-Br_2 can be easily isolated as pure 2,6-diastereoisomers, enabling the synthesis of a regioregular polymeric backbone. Note that isolation of PDIR-Br_2 regioisomers, although demonstrated, is tedious. Therefore, compared to PDIR-based polymers, it should lead to a more π-conjugated structure and, consequently, better charge transport efficiencies. (iii) Proper alkyl (R) functionalization at the rylene nitrogen atoms, in that study 2-octyldodecyl (2OD), should result in highly soluble and processable yet charge transport-efficient polymers. (iv) Finally, the dithiophene (T2) unit is utilized because of the commercial availability, stability, and known electronic structure and geometric characteristics of this core, likely providing highly conjugated, planar, and rod-like polymers. The new NDIR- and PDIR-based polymers were synthesized in high-yields via a Pd-catalyzed Stille polymerization. Using the reported synthetic procedure, polymer M_w values are larger for P(NDI2OD-T2) (**P58**) (~250K, PD ~ 5) than for P(PDI2OD-T2) (**P57**) (~32K, PD ~ 3). The optical and electrochemical properties of these new systems reveal important aspects of the polymer electronic structures and NDIR vs PDIR comonomer effects. Bottom-gate top-contact OTFTs were fabricated on n^{+2}-Si/SiO_2/OTS subsrates on which the semiconducting polymer solutions (~3−10 mg/mL in DCB-$CHCl_3$) were spin-coated to afford ~100 nm-thick films. The films were annealed at 110 °C for 4 h before the TFT structure was completed by Au source/drain vapor deposition. Electrical measurements were performed both under high vacuum and in ambient. Electron mobilities of ~0.08−0.06 cm^2 V^{-1} s^{-1} for P(NDI2OD-T2) and ~0.003−0.001 cm^2 V^{-1} s^{-1} for P(PDI2OD-T2) are measured in vacuum. However, when the same TFT array is measured in ambient, the P(NDI2OD-T2)-based devices continue to function also after 16 weeks from fabrication ($\mu \sim 0.01$ cm^2 V^{-1} s^{-1}), while P(PDI2OD-T2) mobility drops to $\sim 2 \times 10^{-4}$ cm^2 V^{-1} s^{-1} within one week, in agreement with previous studies on PDI-based polymers (Figure 19). In a very recent study we addressed the effect of the regioregularity of these systems by synthesizing the regioregular (only 1,7-linked) P(PDI2OD-T2) as well as the

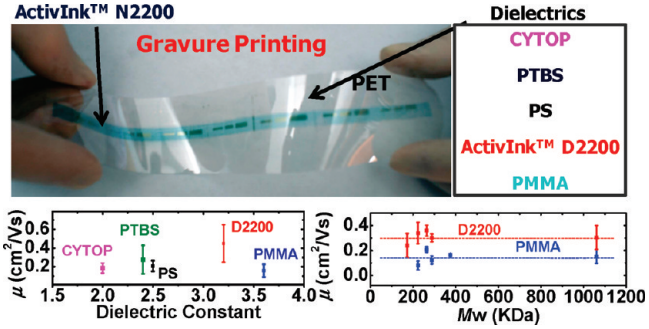

Figure 20. Top. Optical image of the first gravure-printed n-channel polymeric TFTs on a PET web fabricated at Polyera. Center. Mobility vs dielectric constant (k) of the polymeric gate dielectric (left) and molecular weight (M_w) (right). Bottom. Temporal (left) and humidity (right) stability of ActivInk N2200 TFTs with different gate dielectrics.

regioirregular (2,6- + 2,7-linked) P(NDI2OD-T2) polymers. The TFT results show that the regioirregular P(NDI2OD-T2)-based devices exhibit 10× lower electron mobilities, corroborating the key role of the polymer architecture regiochemistry.[79]

The same team also developed high-performance polymeric top-gate bottom-contact (TGBC, Figure 20) TFTs and the first all-polymeric CMOS circuit functioning in ambient based on P(NDI2OD-T2) (**P58**).[80] These TGBC TFTs were fabricated on glass or PET and have the structure substrate/Au(source−drain contacts)/P(NDI2OD-T2)/polymeric dielectric/Au(gate contact). This structure was selected because of the superior injection characteristics of typical staggered (top-gate) architectures and considering the facile channel miniaturization for bottom-contact TFTs which could lead to high-frequency circuits. These devices were fabricated with the P(NDI2OD-T2) film deposited by spin-coating as well as gravure, flexographic, and inkjet printing and with the dielectric layer deposited by spin-coating. Furthermore, TFTs where both the semiconductor and the dielectric layers were gravure-printed are demonstrated. All device fabrication processes were performed in ambient conditions with the exception of the Au contact vapor deposition and the film drying steps (≤110 °C). The TGCB TFTs based on this polymer exhibit excellent n-channel OTFT characteristics in ambient, with electron mobilities up to ∼0.45−0.85 $cm^2/(V\ s)$, $I_{on}:I_{off} > 10^5$, $V_{on} \sim 0-5$ V. Importantly, the carrier mobility of P(NDI2OD-T2)-based TFTs is insensitive to the dielectric constant (k) of the gate dielectric material (Figure 20). This is of great importance to broaden the compatibility of this n-channel semiconductor family with several p-channel materials *using the same gate dielectric*. Furthermore, this polymer's TFT properties are independent of the polymer molecular weight (M_w) over a large range of values ($M_w \sim 200$ KDa to >1 MDa, Figure 20). The insensitivity of the device performance on the polymer chain-length extension is of extreme importance for large-scale synthesis and batch-to-batch reproducibility of the TFT characteristics. P(NDI2OD-T2)-based TFTs are also exceptionally stable in ambient up to ∼70% relative humidity. Due to the stability of this n-channel polymer family, excellent TFT performance with high work-function metal contacts, and compatibility Polyera UV-curable dielectrics with both p- and n-channel semiconductors, they also enabled the first polymeric complementary logic. We have also fabricated printed inverters with P(NDI2OD-T2) (**P58**, n-channel), P3HT (p-channel), and ActivInk D2200 (gate dielectric). These inverters show remarkably small hysteresis reflecting the transistor threshold voltage stability. The voltage gains for the gravure-printed devices are very large ($dV_{OUT}/dV_{IN}(max) > 25-60$). More recently, Noh et al. fabricated monolithically integrated polymeric complementary circuits using P(NDI2OD-T2 and two p-type polymers P3HT and a new dithiophene-based polymer (Polyera ActivInk P2100). Inkjet-printed top-gate/bottom-contact (TG/BC) FETs exhibit very high hole and electron mobilities (μ_{FET}) of 0.2−0.5 $cm^2/(V\ s)$. The FET active regions were patterned and via-holes were defined by direct inkjet printing of the conjugated polymer solutions and the polymer gate dielectric solvent, respectively, enabling high-performance CMOS inverters (gain > 30) and ring oscillators (f_{osc} up to ∼50 kHz).[81]

In a recent paper, Salleo et al. investigated the molecular packing and structure of P(NDI2OD-T2) (**P58**). The importance of molecular packing and microstructure on performance of p-type, thiophene based semiconductors is widely appreciated and has been extensively studied.[82] It is generally believed that the best transport properties are attained when there is a high degree of in-plane π-stacking of the thiophene rings, since this allows for two-dimensional (2D) transport along the chain backbone and along the π-stacking direction in the plane of the substrate.[83] To date, similar structure−property studies are not as well established in n-type polymers due to the dearth of high performing materials. X-ray scattering experiments on P(NDI2OD-T2) films reveal that this polymer exhibits a substantial degree of in-plane ordering and adopts a largely face-on packing (π-stacking direction normal to the substrate), which is an uncommon crystallographic texture for high field-effect mobility semiconducting polymers (Figure 21). Furthermore, we employed X-ray scattering from aligned films as well AFM characterization of the top and bottom interface and, to support these findings, discuss the implications of this unexpected crystalline texture for charge transport.[84]

Finally, recent bulk electron transport by results from both time-of-flight and electron-only current measurements suggest a bulk mobility of $\sim 5 \times 10^{-3}$ $cm^2/(V\ s)$ for **P58**, which is the highest value reported for TOF electron transport in conjugated polymers (Figure 22).[85] Importantly, the electron-only device currents were found to be injection limited for a wide range of electrode work functions and semiconductor layer thicknesses, despite the rather high electron affinity of this polymer. Contact-limited currents were observed even when low work function metals such as Sm, Ca, Ba, or Cs are employed, which are known to enable ohmic contacts with other n-type polymers.[86] However, the previously investigated polymers typically exhibit rather low bulk-transport limited currents owing, for example, to severe electron

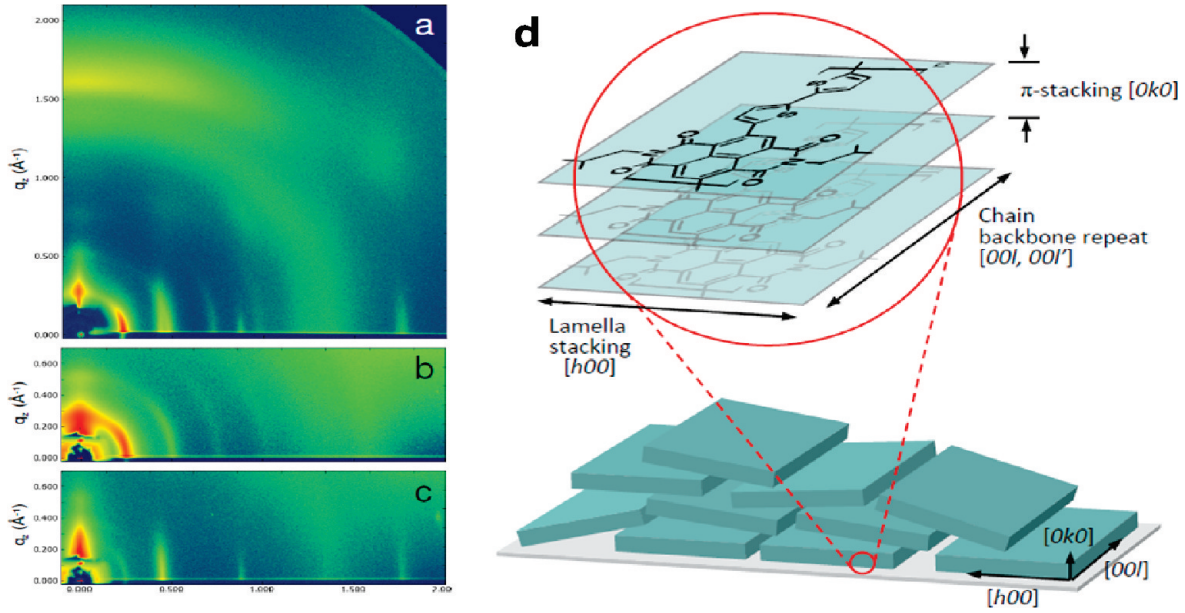

Figure 21. X-ray characterization of P(NDI2OD-T2) structure. (a−c) 2D grazing incidence diffraction pattern from spun cast, isotropic film (a), dip coated, aligned film with scattering vector Q nominally perpendicular to the fiber direction (b), and Q nominally parallel to the fiber direction (c). (d) Schematic of face-on molecular packing of P(NDI2OD-T2) inferred from X-ray data (top) indicating the repeat directions referenced. Proposed microstructural arrangement of the crystallites (bottom) indicating slight disorder in the π-stacking and lamella stacking directions of the flat, platelet-like crystallites. Adapted with permission from ref 84. Copyright 2010 Wiley.

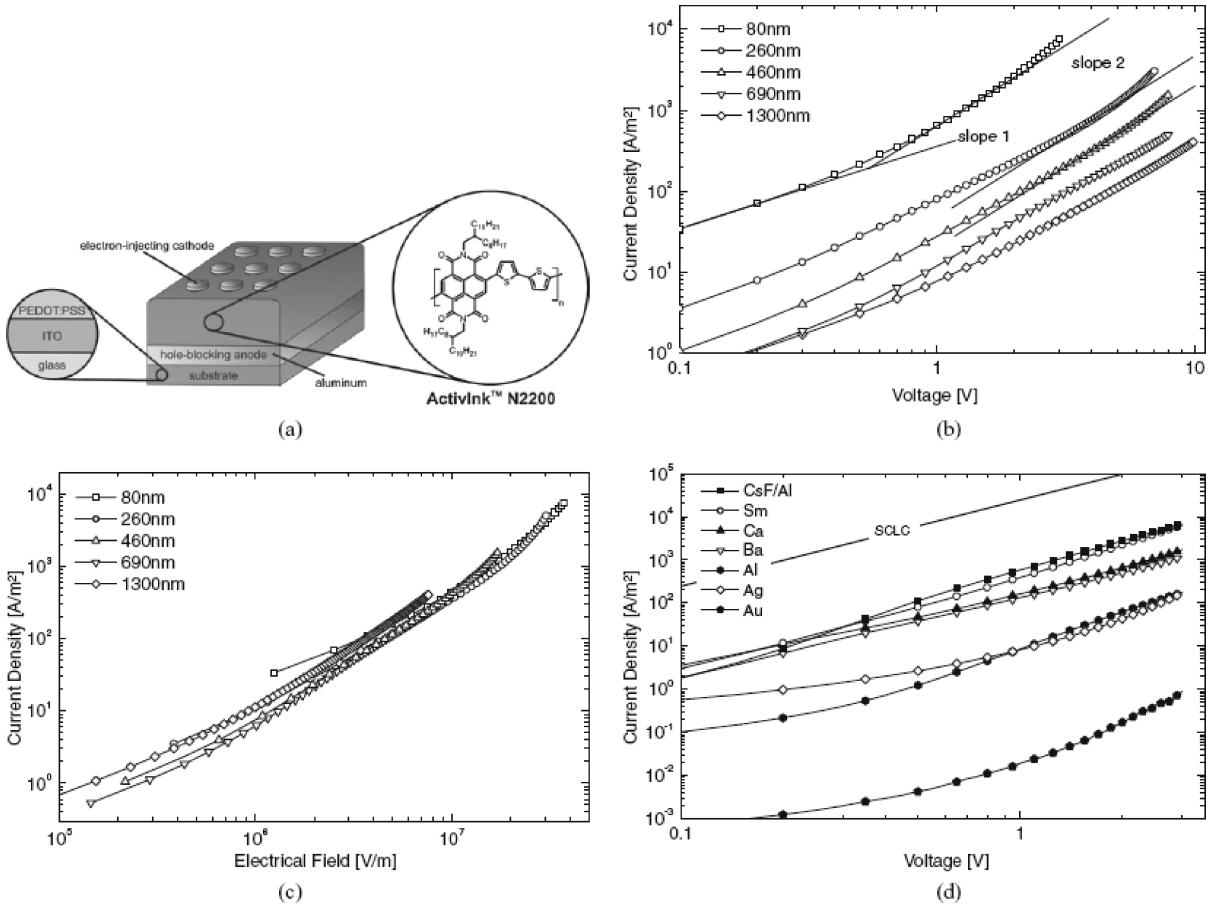

Figure 22. (a) Schematic illustration of an electron-only device used to investigate the charge transport of the conjugated n-type polymer **P58** used in this work. PEDOT:PSS is used as a smoothing layer for the hole-blocking bottom aluminum anode to avoid negative differential resistance effects. (b) $J-V$ characteristics of **P58** electron-only devices with a barium cathode for several N2200 layer thicknesses. (c) $J-E$ characteristics of **P58** electron-only devices with barium cathode for several layer thicknesses. d) $J-$V characteristics of **P58** electron-only devices (d = 85 nm) with different electron-injecting top electrodes. The straight line shows the expected current according to the Mott-Gurney law using the average TOF mobility (μ TOF = 5×10^{-3} cm^2/(V s)). Reprinted with permission from ref 85. Copyright 2010 Wiley.

trapping in an exponential density of states distribution. Thus, we believe that evaporation of reactive metals onto layers of conjugated polymers may commonly cause injection barriers (through the formation of oxides and chemical defects) but that these barriers are masked by the low bulk currents in the majority of n-type polymers that have been investigated to date.

3.4. Ambipolar Polymeric Semiconductors. The vast majority of known organic semiconductors are either hole (p-channel) or electron (n-channel) transporting materials. However, very recently ambipolar organic semiconductors are attracting attention for their potential use in numerous technologically relevant applications.[87] The discovery of ambipolarity as a general characteristic of several semiconducting polymers was made possible by the understanding of the crucial role played by traps of electrons on the surface of several dielectrics, such as hydroxyl, silanol, and carbonyl groups. Representative technological examples are the area of organic microelectronics where patterning of p- and n-channel semiconductors is one of the major hurdles for the implementation of organic complementary logic. In this context, use of ambipolar materials could enable the fabrication of complementary-like circuits through the use of a single semiconductor that functions both as p- and/or as n-channel, hence significantly reducing fabrication complexity.[88] The latest application of ambipolar organic semiconductors is in bifunctional TFTs such as light-sensing (LS-OTFTs) and light-emitting transistors (OLETs).[89] These types of OTFTs can combine electrical switching with additional functionalities such as light sensing or light emission in a single device, making them attractive for various optoelectronic applications including nanoscale light sources and image-sensor arrays.

Ambipolar OFETs based on a number of different materials have been reported. These include thermally evaporated small molecules, spin-coated poly(9,9-dioctylfluorene-*alt*-benzothiadiazole) (F8BT), single crystals of copper and iron phthalocyanines, solution-processed nickel-dithiolenes, and spin-cast squaraines. One of the common features of several ambipolar polymers is the lower bandgap (< 2 eV) compared to the corresponding unipolar semiconductors. This is the result of the typical (but not essential) donor−acceptor-like structure characterized by copolymerization of electron-rich and electron-poor heteroaromatic units. However, despite intensive research in ambipolar organic semiconductors and OFETs, the key material and device properties that enable ambipolar charge transport have been investigated to much less extent than for unipolar charge transport.

Sirringhaus et al. reported the general observation of ambipolar charge transport in a series of regioregular polyselenophene-based polymers.[90] The highest occupied molecular orbital (HOMO) of polythiophenes has little contribution from the sulfur heteroatom, whereas the lowest unoccupied molecular orbital (LUMO) has significant electron density on the heteroatom.[91] Polyselenophenes were initially developed as promising alternatives to polythiophenes for OPV cell applications, mainly because of their reduced optical band gaps. The regioregular polyselenophenes investigated in that work were

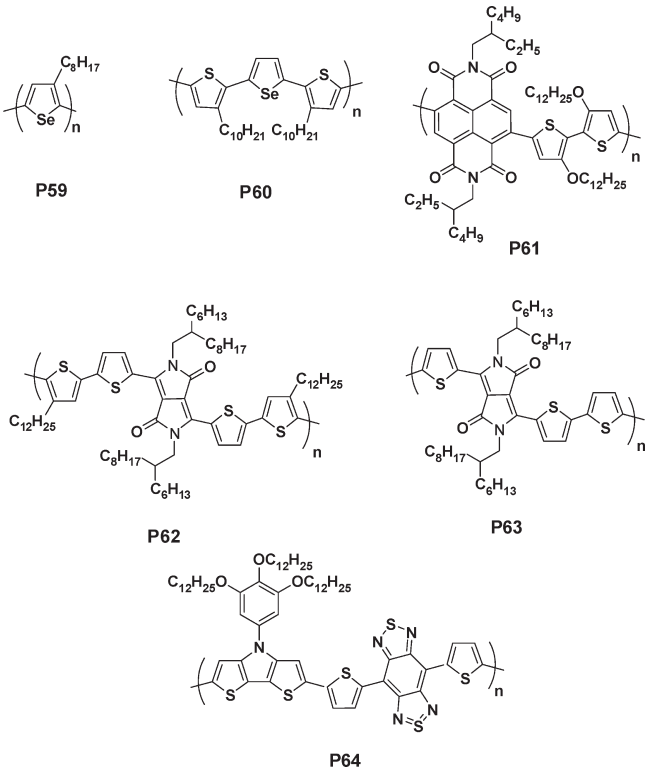

Figure 23. Chemical structure of dithienopyrrole-based p-channel semiconductors **P59**−**P64**.

poly(3,3″-di-*n*-alkylterselenophene) (**P59**) and poly(3-octyl)selenophene (**P60**, Figure 23). Two-dimensional grazing incidence wide-angle X-ray scattering (GIWAXS) indicated that the films were polycrystalline with the side-chain stacking mainly along the out-of-plane direction (perpendicular to the substrate) and $\pi-\pi$ stacking in the in-plane direction. Top-gate, bottom contact (TGBC) TFT configurations with gold source−drain electrodes were employed for all polymers. Polymer **P60** showed clean ambipolar transport characteristics with similar hole and electron saturation and linear mobilities of > 0.01 cm^2/(V s) (PMMA as gate dielectric). While the saturation mobility values for holes and electrons were similar, some reversible hysteresis was systematically observed in the transfer characteristics (Figure 24) in the electron transport regime but not in the hole transport regime, thus indicating the presence of a larger number of shallow traps for electrons than for holes. Using the same device configuration, TFTs based on **P59** exhibited ambipolar properties in as-spun films with hole mobilities of $\sim 0.02-0.09$ cm^2/(V s) and electron mobilities of $\sim 0.004-0.009$ cm^2/(V s). **P60** complementary-like inverter based on two identical TGBC ambipolar transistors with a common gate as input and a common drain as output were fabricated, eliminating the need for semiconductor patterning. The inverting functionality was clearly observed in both the first and the third quadrants, with the input voltage (V_{IN}) and the supply voltage (V_{DD}) being both positively or negatively biased. When V_{IN} and V_{DD} were positively biased, the upper transistor (inset of Figure 24c) was operated in p-channel mode and the lower one operated in n-channel mode, while a reversed situation occurred

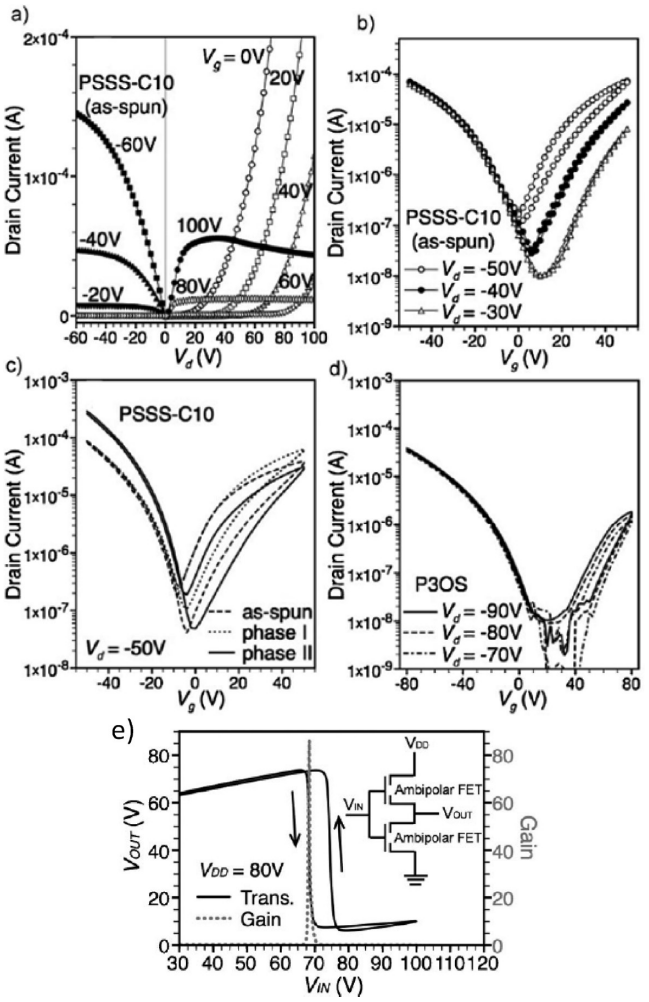

Figure 24. (a, b) The output and transfer characteristics of an as-spun **P60** ambipolar FET with channel length (L) of 40 mm and channel width (W) of 2 cm. The hole and electron mobilities for this device are both ~0.026 cm^2/(V s). (c) Comparison of the transfer characteristics from FETs (L = 20 mm, W = 1 cm) fabricated with **P60** in different phases. (d) The transfer characteristics of an as-spun **P59** ambipolar FET (L = 20 mm, W = 1 mm). All FETs in this figure were fabricated with ~550 nm thick PMMA as the gate dielectric (capacitance C_i = 6.2 nF/cm^2). (e) The transfer characteristic and the corresponding gain (in absolute value) of a complementary-like inverter comprised of two identical as-spun **P60** TGBC ambipolar FETs (L = 20 mm, W = 1 cm). The inset shows the inverter circuit configuration. Adapted with permission from ref 90. Copyright 2010 Wiley.

when the V_{IN} and V_{DD} were negatively biased. The static voltage transfer characteristic (VTC) shown in Figure 24 is typical of inverters made with ambipolar transistors. The observed asymmetry in the threshold voltage, which is higher than $V_{DD}/2$, is related to the asymmetry of the threshold voltages for the p- and n-channel modes, while the hysteresis of VTC is instead due to the hysteresis of the transistor in n-channel mode. Despite the general fact that none of these TFTs can be fully switched off in such an inverter, the authors obtained very high gain in switching (absolute value as high as 86 as shown in Figure 24), which is much higher than the previously reported gain values in inverters composed of ambipolar organic FETs.[92]

Watson and Jenekhe et al. reported a new naphthalene-biscarboximide-bithiophene copolymer semiconductor, **P61**, having an alternating donor−acceptor architecture

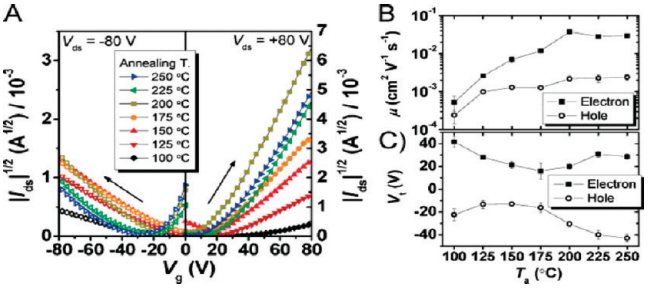

Figure 25. Ambipolar characteristics of **P61**. (A) Square-root of source-drain current versus gate voltage curves at various annealing temperatures (T_a). (B) Saturation mobility and (C) threshold voltage as a function of annealing temperature. Reprinted with permission from ref 93. Copyright 2010 Wiley.

that consists of electron-donating dialkoxybithiophene and electron-accepting naphthalene bisimide.[93] High-mobility ambipolar transistors and high-gain complementary-like inverters were fabricated and exhibit electron and hole mobilities as high as 0.04 and 0.003 cm^2/(V s), respectively, and output voltage gains as high as 30. **P61**-based devices showed typical ambipolar features, such as a diode-like current increase with current saturation at high gate voltage in output curves and V-shape transfer curves with a narrow off-state. However, the film annealing temperature (T_a = 100−250 °C) has notable effects on the ambipolar **P61** transistors. Figure 25A shows the transfer curves of the ambipolar TFTs, $I_{SD}^{1/2}$ versus V_G, as a function of the annealing temperature, T_a. The saturation electron and hole mobilities extracted from these transfer curves are shown in Figure 25B as a function of T_a. As T_a increased from 100 to 200 °C, the mobility increased monotonically from ~5×10^{-4} to ~0.03−0.04 cm^2/(V s) for electrons and from ~2×10^{-4} to ~0.002−0.003 cm^2/(V s) for holes (Figure 25B). About 2 orders of magnitude improvement in electron mobility is observed, while the hole mobility improved by 10×. No significant change in the charge-carrier mobilities was observed for T_a > 200 °C. Unlike the carrier mobility and threshold voltage, the current on/off ratios for the p- and n-channel operation were not affected by the annealing temperature.

Winnewisser et al. report on a new low-bandgap diketopyrrolopyrrole (DPP)-based polymer semiconductor (**P62**) with marked ambipolar charge transport properties.[94] Solution-processed devices using polymeric insulators (PVP or PMMA) and an inorganic gate dielectric (octyltrichlorosilane-treated SiO_2) showed ambipolar behavior. The latter insulator resulted in the highest field-effect mobilities, reaching ~0.1 cm^2/(V s) and up to ~0.09 cm^2/(V s) for holes and electrons, respectively. These values are larger by an order of magnitude than the highest ones previously reported for solution-processed ambipolar transistors. Ambipolarity in this material is not limited to one particular transistor architecture but has been observed in five different configurations including transistors with solution-processed gate dielectrics in bottom-gate as well as top-gate structures. When driven under appropriate bias conditions the ambipolar **P62** transistors

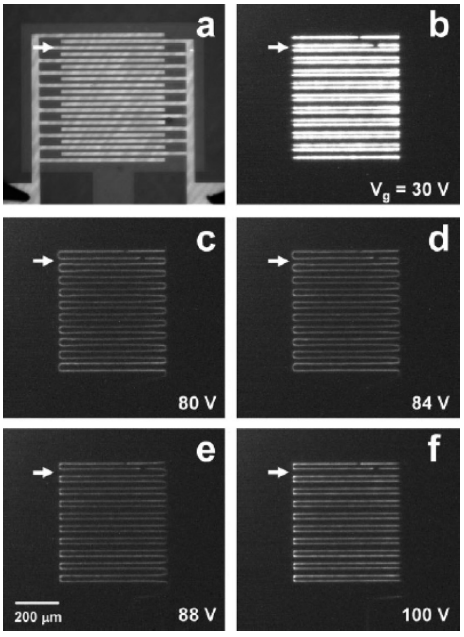

Figure 26. Microscopy images of an operating light-emitting bottom-gate FET. (a) Transistor with interdigitated source−drain electrodes under external illumination. The electrode fingers are 20 mm wide, and the distance between them, i.e., the channel length L, is 10 mm. (b−f) NIR light emitted by the transistor when driven with V_d = 140 V (the drain electrode is the one contacted from the right side) and V_g = 30, 80, 84, 88, and 100 V, respectively. The camera settings were not changed during this series. The white arrow marks the position of the second source finger from the top. Reprinted with permission from ref 94. Copyright 2009 Wiley.

emit near-infrared light, which was the first time that NIR light emission was reported for organic transistors with polymer gate dielectrics as well as for top-gate transistors (Figure 26). A similar structure, **P63**, was reported by Janssen et al. and exhibits ambipolar transport with balanced electron and hole mobilities of ~0.01 $cm^2/(V\ s)$ range, making it an interesting candidate for CMOS-like circuits.[95]

To enable ambipolarity and simultaneously produce soluble low band gap polymers, Reynolds et al. have utilized the strong donor dithieno[3,2-*b*:2′,3′-*d*]pyrrole (DTP) functionalized with a trialkoxyphenyl group, combined with a strong acceptor based on benzo[1,2-*c*;4,5-*c*′]bis[1,2,5]thiadiazole (BBT) to produce the interesting polymer **P64**.[96] This strategy provides a high-lying HOMO, planarity for π stacking, and solubility in the polymers due to the long-chain alkoxy substituents. This polymer is spray-processable and shows an optical bandgap of only 0.5−0.6 eV, which is the lowest value reported for a soluble polymer. In electrochemical cells, four differently colored redox states of the polymer can be accessed at moderate potentials and have good stability. This polymer also shows potential for use in ambipolar OFETs with respectable mobilities of 1.2×10^{-3} and 5.8×10^{-4} $cm^2/(V\ s)$ being measured for p-channel and n-channel operation, respectively.

Finally, Loi et al.[97] have demonstrated high performance organic ambipolar TFTs based on blends of P(NDI2OD-T2) (**P52**)/P3HT (**P1**) as the semiconductor layer. The two polymers form a type-II heterojunction, also resulting in the photogeneration of charges as shown by time-resolved

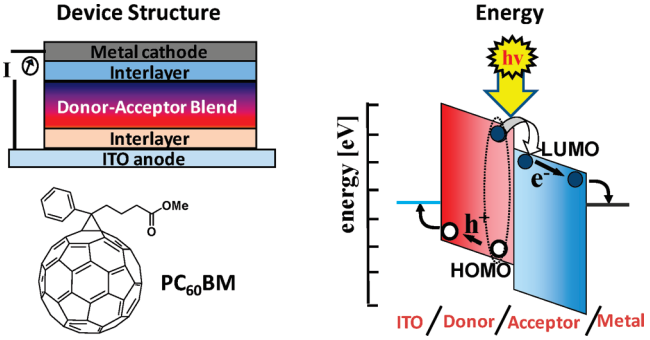

Figure 27. Structure and materials of a conventional bulk-heterojunction photovoltaic cell along with the energy levels of the materials where light absorption/excition dissociation/charge collection takes place. The chemical structure of $PC_{61}BM$ is also shown.

photoluminescence measurements. The devices fabricated in bottom contact bottom gate configuration exhibit balanced electron and hole charge carrier mobilities. The extracted values were 4×10^{-3} $cm^2/(V\ s)$ for electrons and 2×10^{-3} $cm^2/(V\ s)$ for holes with I_{on}/I_{off} ratios of ~10^3, which are the highest reported so far for polymer bulk heterojunction-based TFTs. The large ambipolarity and optical characteristics of this bulk heterojunction may hold promise for future opto-electronic applications.

4. Bulk-Heterjunction Photovoltaic Cell Applications

Conversion of solar energy into electrical power is a renewable clean energy.[98] Bulk-heterojunction organic photovoltaic (BHJ OPV) cells are a potential competitor to amorphous silicon-based technologies and have experienced tremendous progress in performance during the last three years, with power conversion efficiency (PCE) now routinely surpassing 8%.[99] Bulk-heterojunction cell photoactive layer is composed of a blend of bicontinuous and interpenetrating donor (hole-transporting) and acceptor (electron-transporting) semiconductors (Figure 27).[100] In a typical BHJ OPV cell, the photoactive blend layer is sandwiched between an indium tin oxide (ITO) positive electrode (anode) and a metal negative electrode (cathode). Organic and/or inorganic interlayers are also used to improve hole collection to the anode (e.g., PEDOT:PSS) and electron collecting to the cathode (e.g., LiF). In a typical polymeric cell a low band gap conjugated polymer donor and a soluble molecular acceptor are used.[101] Typical acceptors are soluble fullerene derivatives such as [6,6]-phenyl-C61-butyric acid methyl ester ($PC_{61}BM$). As a component in the active layer, a conjugated polymer donor serves as the main absorber to solar photon flux, as well as the hole transporting phase.[102] Therefore, wide optical absorption to match the solar spectrum and large hole (bulk) mobility are basic requirements to design an ideal polymer donor. Furthermore, microstructural features such as charge transport maximized in the out-of-plane direction is a desirable characteristic.

Compared to bilayer OPV structures, in BHJ-OPV architectures the donor phase is intimately intermixed with the acceptor phase and thus the excitons can more

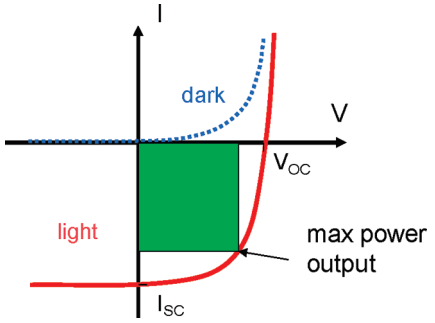

Figure 28. Schematic of the $I-V$ curve in the dark and under illumination of an OPV cell.

easily access the donor−acceptor interface and subsequently dissociate to free holes and electrons. The charge carriers will then easily move to the corresponding electrodes by following the continuous route of either donor or acceptor phases. Thus a mixed layer of donor and acceptor molecules sandwiched between homogeneous donor and acceptor layers can have significantly improved device performance compared to donor−acceptor bilayer cells. Polymer-based cells have the advantage of avoiding the high cost of small-molecule coevaporation, as well as compared to soluble molecular semiconductors, they result in uniform films over large area greatly facilitating roll-to-roll (R2R) production.

From the photocurrent spectrum it is possible to derive the ability of the solar cells to convert photons to electrons under irradiation at certain wavelengths and intensities, providing the reference of the photon to electron transfer capability of the solar cell. However, among the most important performance parameters there are the power conversion efficiency (PCE or η) and the open circuit voltage (V_{oc}), which can be extracted from the solar cell $I-V$ curves measured under the simulated AM 1.5 solar light (Figure 28). Thus, the overall PCE is calculated according to the following equations:

$$\eta = P_{out}/P_{in} = \mathrm{FF}(V_{oc}I_{sc})/P_{in} \quad (3)$$

$$\mathrm{FF} = (V_{mpp}I_{mpp})/(V_{oc}I_{sc}) \quad (4)$$

where P_{out} is the maximum output electrical power (in W/m^2) of the device under illumination, P_{in} (in W/m^{-2}) is the light intensity incident on the device, V_{oc} is the open circuit voltage, and I_{sc} is the short circuit current in A/m^{-2}. Other important parameters which can be extracted from the photocurrrent−photovoltage plots are the short circuit current (J_{sc}) and the fill factor (FF). J_{sc} is the current extracted from the device under illumination when no bias is applied. The parameter FF is defined as where V_{mpp} and I_{mpp} are the voltage and current at the maximum power point in the $I-V$ curve, respectively.

An ideal device would have a rectangular shaped $I-V$ curve and therefore a fill factor FF approaching unity. The overall efficiency is an important parameter for evaluating the performance of the device and is the default efficiency value mentioned in the literature. Note

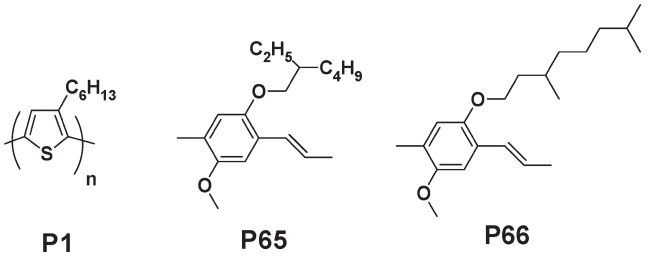

Figure 29. Chemical structure of the traditional donor polymers **P1**, **P65**, and **P66**.

that besides experimentally characterizing the performance of the organic solar cells, a key parameter, the V_{oc}, can be estimated from electrochemical measurements and given by the difference between the donor HOMO level and the acceptor LUMO level. It is now well-accepted that for a given acceptor V_{oc} correlates linearly with the donor HOMO level and vice versa. For example, in the case of polymer: $PC_{61}BM$-based solar cells, the V_{oc} value can be estimated by $V_{oc} \sim E_{LUMO(Acceptor)} - E_{HOMO(Donor)} - 0.3$ V, where the constant 0.3 V is due to the difference between the HOMO/LUMO energy levels and the electrochemical potential at which the charges are extracted from the device. Clearly, to achieve an organic BHJ-PV cell with large power conversion efficiency and stability, the materials have to be designed carefully to fulfill key parameters such as HOMO/LUMO energy levels, solar light absorption, and blend morphology/microstructure to maximize light absorption, charge separation, and charge transport/collection.

4.1. Donor Polymeric Semiconductors. Traditional π-conjugated polymers used as donor semiconductors in OPV cells are shown in Figure 29. Dialkoxy-substituted poly(para-phenylene vinylene)s **P65** and **P66** exhibit strong absorption in the visible light band[103] and PCE values of > 3% have been reported. Regioregular poly(3-hexylthiophene) (**P1**) has also been widely investigated with record PCEs > 6% when proper acceptors are used.[104] To enhance of OPV cells based on P3HT (**P1**), MEH-PPV (**P65**), and MDMOPPV (**P66**), several optimization strategies have been employed such as using solvent mixtures/additives, photoactive layer thermal annealing/film forming conditions, optical spacer, anode/cathode interfacial layers, and using different device architectures.[105]

For instance, Marks and co-workers have utilized organic and inorganic interlayers to improve OPV efficiency using **P66** and **P1** as testbeds. Among the factors limiting V_{oc}, there is the risk where both phase-separated donor and acceptor components can be in electrical contact with *both* electrodes. Thus, electrons transported by the $PC_{61}BM$ network may drift/hop to the ("wrong") hole-extracting ITO anode. Such efficiency-depleting phenomena are well-established for OLEDs/PLEDs.[106] While for OPVs this leakage current flow opposes the built-in electric field, it is favorable for an electron in the $PC_{61}BM$ LUMO (~4.0 eV) to transfer to ITO (work function ~ 4.7 eV). Electrons transferred to the ITO would then recombine with holes to erode device efficiency and reduce the maximum possible V_{oc}. Thus, an

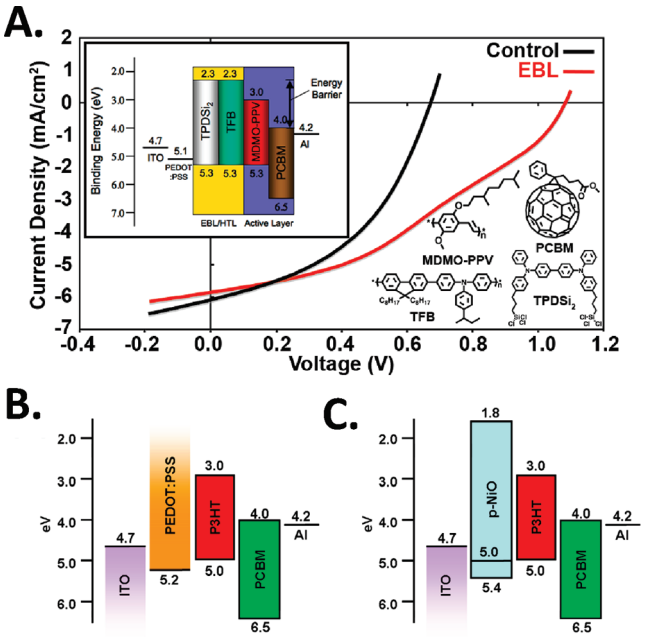

Figure 30. (A) $J-V$ plots for **P66** + $PC_{61}BM$ BHJ cells fabricated with and without (control) a 15 nm electron-blocking layer (EBL). V_{oc} increases from ~0.70 to 1.08 V and η_p increases from 1.7% to 2.5% upon insertion of the EBL. Inset: OPV component energy levels. The energy barrier to electron flow in the wrong direction is shown. (B) Energy levels of a P3HT (**P1**)-$PC_{61}BM$ cell with a PEDOT-PSS hole injection/electron-blocking layer. (C) Energy levels of a P3HT-$PC_{61}BM$ cell with a NiO hole injection/electron-blocking layer. Adapted with permission from ref 109. Copyright 2008 National Academy of Sciences.

OPV cell model consisting of **P66** + $PC_{61}BM$ cell (Figure 30) was fabricated with and without an organic interlayer. Marks et al. found that a $TPDSi_2$ + TFB cross-linked electron-blocking layer (EBL) chemisorbed between the active layer and the anode produces a record V_{oc} = 1.08 V for a materials system having a theoretical maximum V_{oc} ~ 1.2 V (Figure 30).[52,53] This interfacial layer substantially increases PCE and thermal stability.[107] In a different approach, the same group used NiO as an inorganic interlayer to fabricate P3HT-based cells. NiO is a transparent conducting p-type oxide, and considering the relevant energy levels for P3HT + $PC_{61}BM$ cells indicates that a thin layer of NiO on the ITO anode could enhance hole extraction while blocking electron leakage to the anode. Both NiO and ITO are wide-band gap transparent conducting oxides to the P3HT-PCBM materials. The highest PCE reported at the time for optimized P3HT-$PC_{61}BM$ cells, using standard fabrication procedures, were ~4.0% efficiency.[108] Using the same fabrication procedure, NU used a thin (5 −70 nm) NiO films grown on ITO anodes by PLD (pulsed laser deposition) and P3HT + $PC_{61}BM$ cells fabricated on top of this anode. For optimum NiO thicknesses of 5−10 nm, the NU team achieved record cell power efficiencies of 5.2% (NREL measured 5.6%)[109] Importantly, control experiments with n-type TCOs both at NU and elsewhere do not show this effect which is attributable, among other factors, to the good hole transport characteristics of NiO. Note that the greatest effect of the NiO layer was to increase the fill factor and V_{oc}.

Studies on the above-mentioned polymers paved the way to understanding how bulk-heterojunction OPV cell function and what the critical parameters affecting efficiency and stability are and identified routes to design even better donors. However, significant PCE improvement is necessary to meet large scale commercialization requirements. Thus, during the last three years several π-conjugated polymers were identified as promising donor candidates, and due to the limited space, we will concentrate only on a few of them. Key routes toward better donor polymers are to enlarge their optical absorption to better match the solar terrestrial radiation, enhance (bulk) hole mobility, and improve energy alignment with the acceptor to enhance the open circuit voltage.

The synthetic strategy to reduce the bandgap and broaden the optical absorption is to realize alternating copolymers comprising electron-rich (donor) and electron-deficient (acceptor) heteroaromatic units.[110] Among the donating groups there are dithiophene, cyclopentadithiophene, carbazole, dibenzo(thieno)silole, fluorene, and dialkoxybenzodithiophene, whereas the acceptors are benzothiadiazole, quinoxaline, thienoimide (thieno[3,4-*c*]pyrrole-4,6-dione), and diketo-pyrrolo-pyrrole (DPP), to cite just a few.

Cyclopentadithiophene-benzothiadiazole copolymer **P67** has been reported by Brabec et al. in a series of papers.[111] **P67** exhibits a high hole mobility of 2×10^{-2} $cm^2/(V\ s)$, a wide absorption band at ~750 nm, and a low E_g of 1.4 eV. The HOMO and LUMO levels of **P67** are −5.3 and −3.57 eV, respectively. With $PC_{61}BM$ and $PC_{71}BM$ (1:1 by weight) **P67** exhibits PCEs of 2.67% and 3.16%, respectively. When additives (e.g., 1,8-octanedithiol) were used during photoactive layer deposition to the active layer, PCEs of 5.1−5.5% were achieved. The enhanced PCE was attributed to increased mobile-carrier-generation efficiency and mobile-carrier lifetime. The corresponding dithienosilole-BT alternating copolymer, **P68**,[112] reported by Yang et al., exhibits a broad absorption extending to 800 nm, an E_g of 1.45 eV, and a FET hole mobility of 3×10^{-3} $cm^2/(V\ s)$. With an active layer of **P68a**:$PC_{71}BM$ (1:1 by weight), OPV devices showed an outstanding PCE of 5.1%. Boudreault et al.[113] and Wang et al.[114] independently reported the dibenzosilole-BT copolymer **P68b**. The first group synthesized the polymer having M_n/M_w = 15/20 KDa, whereas the second group achieved M_n/M_w = 79/330 KDa. The shorter M_w version exhibits lower OPV performance characterized by a J_{sc} of 2.80 mA/cm^2, V_{oc} of 0.97 V, and FF of 55% under illumination at 90 mW/cm^2, giving a PCE of 1.6% (1:1 weight ratio with $PC_{61}BM$). The FET hole mobility for **P68b**, measured under ambient conditions without any encapsulation, reached ~10^{-3} $cm^2/(V\ s)$. The much higher molecular weight **P68b** batch afforded greater photovoltaic performance with PCE of ~5.4%, from the same device configuration but with a different component ratio (**P68b**:$PC_{61}BM$ = 1:2 by weight). More recently, Jen et al. reported two novel low-bandgap copolymers (**P69**) based on the benzobis(silolothiophene) unit.[115] The polymers exhibit high hole mobilities (up to 0.01 $cm^2/(V\ s)$) and power conversion efficiency of ~3.5%.

Fused coplanar thiophene-based heterocycles have been actively utilized as both donor and acceptor units.

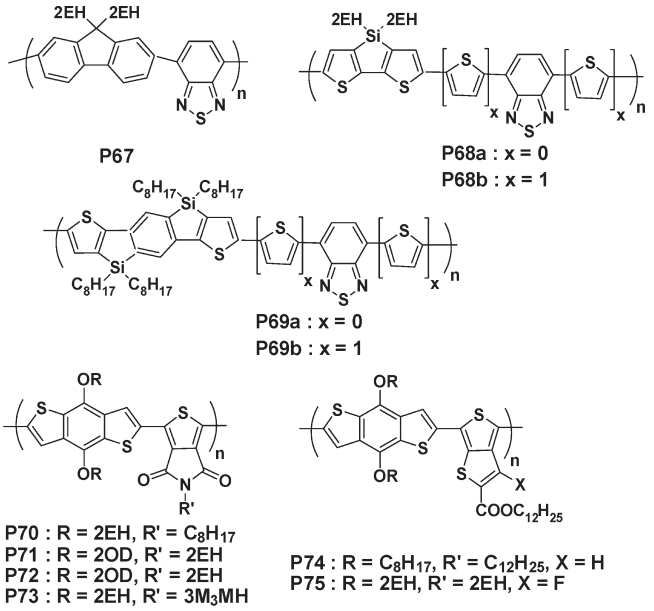

Figure 31. Chemical structure of donor polymers **P67**−**P75**.

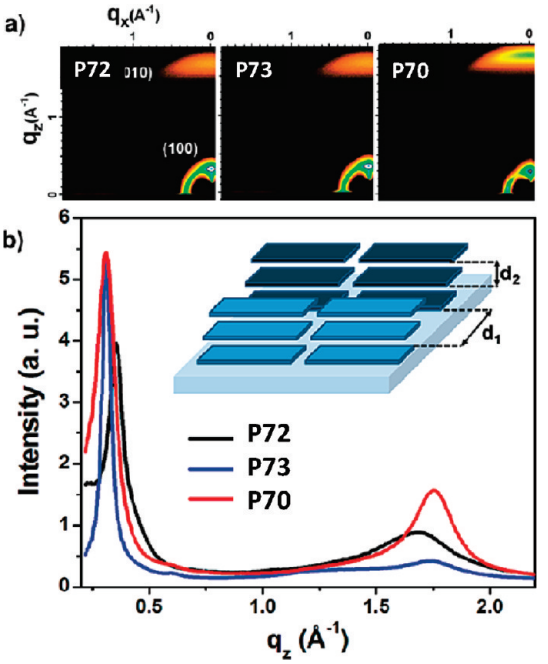

Figure 32. (a) 2D grazing incidence X-ray scattering (GIXS) patterns of films of **P72**, **P73**, and **P70**. (b) Out-of-plane linecuts of GIXS. Inset: Schematic illustration of the face-on orientation of the polymers with the backbone parallel to the substrate. The lamellar spacing and the π-stacking distance are labeled d_1 and d_2, respectively. Adapted with permission from ref 120. Copyright 2010 American Chemical Society.

Leclerc et al. explored the used of the thieno[3,4-*c*]pyrrole-4,6-dione (TPD) unit[116] in combination with alkoxy-benzodithiophene (TBT) to realize a very interesting copolymer (**P70**, Figure 31).[117] TPD is a very simple, easy to synthesize, planar structure, and considering its relatively strong electron-withdrawing effect lead to low HOMO and LUMO energy levels, which are desirable to increase V_{oc}. **P70** is readily soluble in chlorinated solvents upon heating and exhibits a M_n of 13 kDa and M_w of 34 kDa (TCB at 140 °C). The optical band gap obtained from this polymer film absorption edge is 1.8 eV. Interestingly, the UV−vis absorption of **P70** in solution is very similar to that obtained in the solid state, indicating a similar rigid-rod conformation in both states. The HOMO and LUMO energy levels are −5.56 and −3.75 eV, respectively, on the basis of the onset of the oxidation and reduction currents. The photovoltaic properties of **P70**-$PC_{71}BM$ (weight ratio of 1:2) were investigated in an OPV structure consisting of ITO/PEDOT:PSS/**P70**:$PC_{71}BM$/LiF/Al, having an active area of 1.0 cm^2. These devices demonstrated a short-circuit current density of 9.81 mA/cm^2, a V_{oc} of 0.85 V, a fill factor (FF) of 0.66, and a PCE of ∼5.5%. Note that efficiencies obtained on areas smaller than 0.2−0.3 cm^2 may become strongly size-dependent.[118] Structures based on the same TPD-TBT-building blocks, but having different alkyll chains, were reported independently by Xie et al.[119] Thus, **P71** was synthesized and the morphologies of **P71**:$PC_{71}BM$ blend films were optimized by the addition of diiodooctane resulting in PCE of 4.79% and V_{oc} of 0.91 V. More recently, **P70** and two other TPD-TBT polymers (**P72** and **P73**) were reported by Frechet et al. and identified device configurations yielding PCEs between 4% and 6.8%.[120] The photovoltaic properties of these polymers were investigated with $PC_{61}BM$. The active layers were spin-coated from chlorobenzene (CB) and, in some cases, a small amount of the high boiling-point additive 1,8-diiodooctane (DIO). In optimized devices, the PCE increases from 3.9% for **P72**, which possesses an ethylhexyl side chain, to 5.4% for **P73**, which possesses a dimethyloctyl side chain. The elimination of branching on the TPD side chain in **P70** further enhances PCE performance to 6.8%. In the cases of **P72** and **P73**, the addition of DIO to the blend solution dramatically improved the device performances. It is known that the use of high-boiling-point additives promote polymer packing by avoiding excessive crystallization of the fullerene.[121] The authors showed that this mechanism is responsible for the large enhancement in the device performances of **P72** and **P73**. In contrast, for devices realized using P70, the addition of DIO led to only slight improvements, suggesting that **P70** blend morphology optimizes without DIO addition. The authors studies microstructural organization by grazing incidence X-ray scattering (GIXS). As shown by the GIXS patterns of **P72**, **P73**, and **P70** (Figure 32a), the (010) peak corresponding to π-stacking is more prominent in the out-of-plane direction, which suggests that most of the polymer backbones are oriented parallel to the substrates (inset, Figure 32b). This face-on orientation is beneficial for charge transport in the device. Interestingly, the same diffraction peaks of the pristine polymers are still visible in the 2D patterns of the blends with $PC_{61}BM$ together with the characteristic reflection of fullerene.

Following the first study of Yang et al.[122] where several alkoxy-benzodithiophene-based polymers were synthesized, Yu et al. reported[123] an alkoxy-benzodithiophene-*co*-thienothiophene polymer **P74** with a low E_g of ∼1.6 eV exhibiting PCE of 5.6% for devices fabricated with $PC_{71}BM$ as the acceptor. The hole mobility of **P74** was

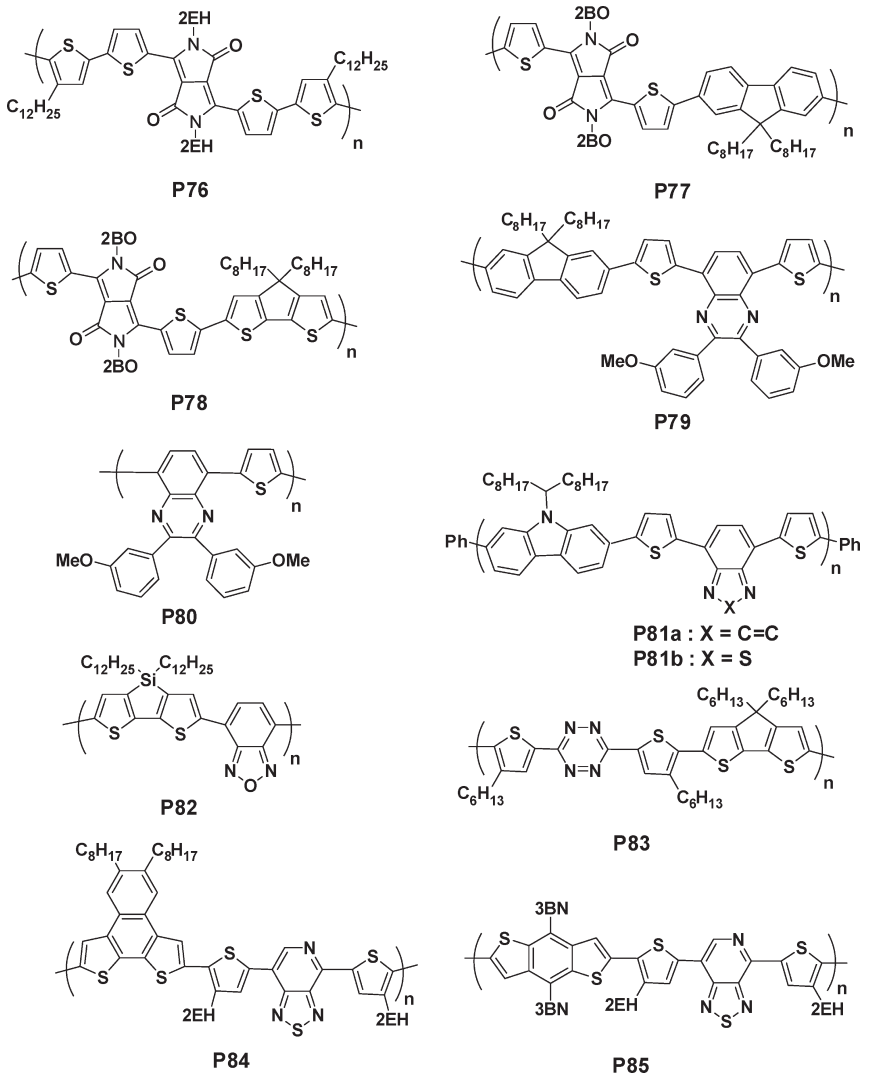

Figure 33. Chemical structure of donor polymers **P76**−**P85**.

10^{-4} $cm^2/(V\ s)$. More recently the same group reported a variation to the same structure where a F atom was included in the thiophene ring (**P75**).[124] The M_w of **P75** is 97.5 kDa with a polydispersity index of 2.1 whereas the HOMO and LUMO energy levels are −5.15 eV and −3.31 eV, respectively. Despite the branched chains, the space −charge limited current hole mobility approaches 10^{-3} $cm^2/(V\ s)$. This polymer shows strong absorption from 550 to 750 nm. An impressive PCE of ∼7.4% has been achieved when $PC_{71}BM$ is used as the acceptor.

Small band gap conjugated copolymers[125] and oligomers[126] were also realized by incorporating diketo-pyrrolopyrrole (DPP) with the appropriate electron-rich aromatic groups, resulting in materials with interesting OPV performance (Figure 33). Thus, Janssen et al. introduced the diketo-pyrrolo-pyrrole into the backbone of polythiophene resulting in the polymer **P76**, which exhibits a band gap of only 1.4 eV.[127] The polymer was very soluble in chloroform but partially soluble in *o*-dichlorobenzene. Using a mixture of the two solvents to dissolve **P76** and $PC_{71}BM$ resulted in OPV efficiencies of ∼4%. More recently the same group reported new polymers incorporating diketo-pyrrolopyrrole with different electron-rich aromatic segments such as 9,9-dioctylfluorene (**P77**) and 4,4-dioctylcyclopenta[2,1-*b*:3,4-*b*0]dithiophene (**P78**). These polymers exhibit solid-state band gaps ranging from 1.24 to 1.77 eV. In field-effect transistors ambipolar charge transport with hole and electron mobilities of $\sim 10^{-3}$ and 10^{-4} $cm^2/(V\ s)$, respectively, were measured. Bulk heterojunction OPV cells were fabricated with $PC_{61}BM$ as the electron acceptor to give a maximum power conversion efficiency of 1.7% under simulated standard solar light (AM1.5G, 100 mW/cm^2). The authors claimed that the bulk heterojunction blend morphology limits OPV performance.

An interesting electron-poor heterocycle used in OPV polymer is quinoxaline. Inganas et al. reported the alternating copolymer **P79** formally derived from fluorene and 5,8-dithienylquinoxaline.[128] This polymer has an E_g of ∼1.9 eV and a very low-lying HOMO of −6.3 eV, and OPV cells fabricated with PC60BM exhibit PCEs of 3.7%. Similar quinixaline-based derivatives exhibit PCEs between 1.1 and 2.7%,[129] and a recent derivative **P80** has shown even greater potential.[130] Copolymer **P81a** obtained by Leclerc et al. by combining 5,8-dithienylquinoxaline with 2,7-carbazole exhibits an E_g of 2.02 eV and a TFT

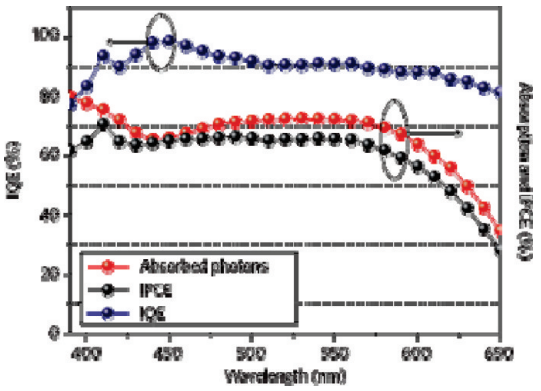

Figure 34. Internal quantum efficiency (IQE) of **P81b**:$PC_{71}BM$ solar cells. (a) IQE values of the 1:4 device with film cast from DCB. The red line shows the total absorption of the device, and the black line the IPCE. Adapted with permission from ref 132. Copyright 2009 Nature Publishing Group.

hole mobility of 3×10^{-4} cm2/(V s).[131] Within the same study, structural variations were also explored where pyrido-pyrazine (**P81a**) and benzothiadiazole (**P81b**) replaced quinoxaline, resulting in PCEs of ~1−2%. Lee and Heeger used the Leclerc polymer **P81b** polymer with $PC_{71}BM$ to fabricate solar cells exhibiting excellent performance with PCE surpassing 6%.[132] To increase the photocurrent while maintaining the thickness constant, they used an optical TiO_x spacer[133] between the photoactive layer and the top electrode; because of the optical spacer, the maximum light intensity is redistributed to be within the active charge separating the BHJ layer. In parallel, by choosing optimal conditions for processing, they demonstrated a nanoscale BHJ morphology resulting in nearly 100% internal quantum efficiency (IQE), meaning that every photon adsorbed in the photoactive layer is collected as electron/hole at the corresponding contacts (Figure 34). Bazan et al. introduced a novel donor polymer, namely, poly[(4,4-didodecyldithieno[3,2-*b*:20,30-*d*]silole)-2,6-diyl-*alt*-(2,1,3-benzoxadiazole)-4,7-diyl] (**P82**).[134] The idea was that due to the benzoxadiazole for benzothiadiazole substitution, larger open-circuit voltages should be achieved. The M_w of **P82** is 41 KDa, and the HOMO and LUMO are −5.5 and −3.7 eV, respectively. Solar cells were fabricated using **P82** and $PC_{71}BM$ as the acceptor in a 1:2 weight ratio and exhibit maximum PCEs approaching 2%.

Very recently, Ding and co-workers reported a new s-tetrazine-based low-bandgap semiconducting polymer (**P83**), which is the first solution-processable conjugated polymer with tetrazine in the main chain. This polymer shows good thermal stability, broad absorption covering 450−700 nm, and HOMO and LUMO energy levels of −5.34 and −3.48 eV, respectively. Solar cells fabricated with $PC_{71}BM$ exhibit power conversion efficiency of ~5.4%.[135] Finally, You et al. synthesized a series of weak donor−strong acceptor polymers, **P84**−**P85**, copolymerizing various donor moieties with thiadiazolo[3,4-*c*]pyridine. These new polymers showed noticeably reduced LUMO levels, slightly decreased HOMO levels, and thus smaller bandgaps than the corresponding 2,1,3-benzothiadiazole.

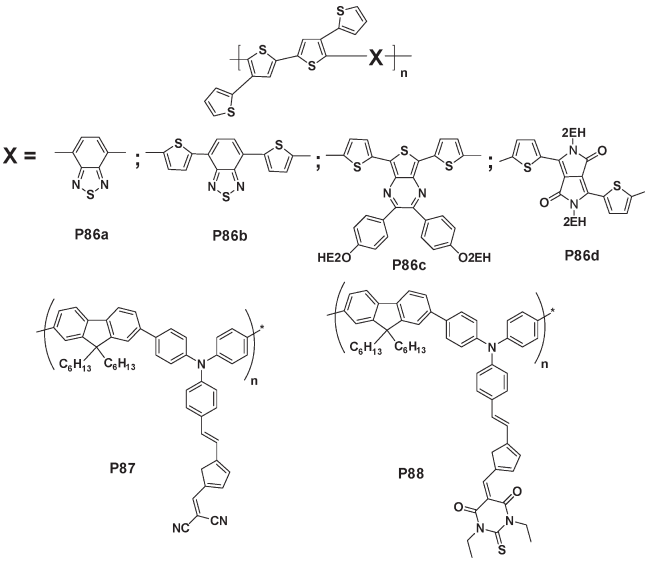

Figure 35. Chemical structure of donor polymers **P86**−**P88**.

The smaller bandgap significantly improves the observed J_{sc} values of the related BHJ devices, while the low HOMO energy level maintains the high V_{oc} values. BHJ photovoltaic devices were fabricated with a typical configuration of ITO/PEDOT:PSS(40 nm)/polymer:$PC_{61}BM$/Ca(40 nm)/Al(70 nm) and tested under simulated air mass coefficient AM1.5G illumination, resulting in efficiencies > 6%.[136]

Most of the above-reported donor−acceptor conjugated copolymers focused on the main chain system. Recently, two-dimensional (2D) like conjugated polymers with conjugated side chains have been developed by several groups (Figure 35).[137] Pioneering works done by Li and his co-workers concluded that the incorporation of conjugated side chains into polythiophene significantly broadened the absorption spectrum and enhanced the power conversion efficiencies of photovoltaic cells, such as bi(phenylenevinylene), bi(thienylenevinylene), and phenothiazinevinylene. In addition, the cross-linked polythiophene derivatives with conjugated bridges were shown to have high charge carrier mobility. Unlike the bi(thienylenevinylene) system, Ting et al. employed the alkylthiophenes directly attached onto the polythiophene backbone without the vinylene linkers.[138] Such polymers have a far lower band gap of 1.77 eV and relatively low-lying HOMO levels (−5.46 to −5.62 eV) versus P3HT, indicating improved absorption ability and air stability. Very recently, similar structures with less densely conjugated side chains compared to their previous study exhibited hole mobility of ~0.05 cm^2/(V s). These copolymers showed interesting OPV efficiencies. The above reports suggest that 2D-like conjugated polymer systems have emerged as a promising candidate for the donor building block. More recently, Ting reported the synthesis, properties, and optoelectronic device applications of the four poly(4T-acceptor) derivatives (**P86a**−**d**, Figure 35).[139] Polymer solar cell devices were fabricated by spin-coating the polymer blend of 4T-acceptor copolymer/$PC_{71}BM$ sandwiched between a transparent anode (ITO) and

cathodes (Ca/Al). The high hole mobilities of these polymers (10^{-1}−10^{-4} $cm^2/(V\ s)$) are mainly due to the enhanced ordered intermolecular packing characteristics in the solid state. The power conversion efficiencies of **P86a**−**d** are as high as 2.43%. Very recently, Jen et al. used the same concept and synthesized side chains polymer series where **P87** and **P88** are two representative examples. Different from the common linear donor−acceptor conjugated polymers, in **P87** and **P88** the acceptors are located at the ends of the side chains and connected with the triphenylamine donors on the main chain through a styrylthiophene π-bridge. Hence, the designed polymers have an electron-rich conjugated main chain with a D-π-bridge-A conjugated side chain. This new design takes advantage of the group of well-established knowledge of nonlinear optical chromophores to optimize the absorption spectra and energy levels of the resultant polymers.[140] **P87** and **P88** exhibit a high hole mobility of $\sim$0.01 $cm^2/(V\ s)$, and OPV cells with PC61BM and PC71BM exhibit promising performance with maximum PCEs approaching 5%.

4.2. Acceptor Polymeric Semiconductors. Fullerenes are by far the most used and technologically relevant OPV acceptors.[141] However, fullerenes suffer several drawbacks such as batch to batch performance variations, limited availability, and unstable active layer morphology of the corresponding blends. Despite the lack of well-understood rules on how to design efficient acceptor semiconductors for OPV, several groups have initiated the search for alternative donors based on small-molecule and polymeric materials.[142] Unfortunately from these studies one of the results is that high-performance electron-transporting TFT semiconductors[143] do not exceed as OPV acceptors.

The polymeric acceptor poly[2-methoxy-5-(2′-ethylhexyloxy)-1,4-(1-cyanovinylene)phenylene] (CNPPV, **P89**) was first investigated in OPV devices by Friend and coworkers in 1998 (Figure 36).[144] By combining this polymeric acceptor with poly[3-(4-*n*-octyl)-phenylthiophene] (POPT),[145] that study proofed the concept of bulk-heterojunction as a means to improve efficiency on organic solar cells using all polymeric materials and yielded the highest photocurrent of its time with peak EQE of 28%.

Very recently, Frechet et al.[146] synthesized a high-quality POPT via GRIM resulting in a high M_n and regioregular polymer which afforded a peak efficiency of 3.1% with $PC_{61}BM$. More importantly, thanks to the high solvent resistance of GRIM POPT, **P89** can be spin-coated directly on top of a POPT film using solvents such as tetrahydrofuran or ethyl acetate, leading to bilayer devices as opposed to the previously laminate design explored by Friend. A peak efficiency of 2.0% was achieved with this system after 2 h of thermal annealing at 110 °C. This constitutes among the highest reported efficiency to date for a solution processed all-polymer OPV.[147] Li et al. report all-polymer OPV cells based on a polymer blend of poly-3,10-*n*-octyl-3-phenothiazine-vinylenethiophene-*co*-2,5-thiophene as donor and poly-1,4-dioctyloxyl-*p*-2,5-dicyanophenylenevinylene (**P90**) as

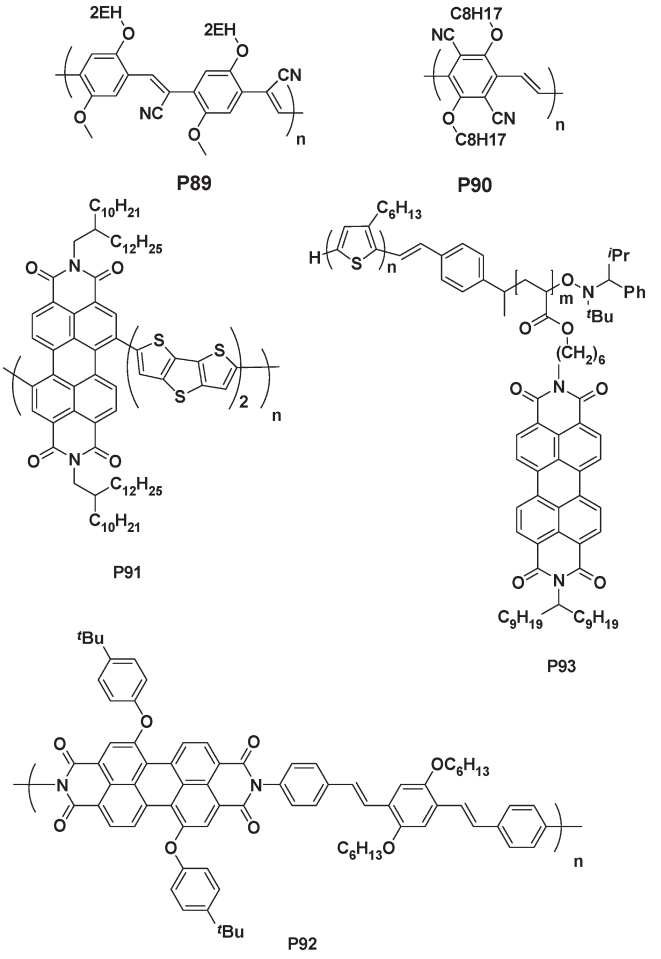

Figure 36. Chemical structure of donor polymers **P67**−**P75**.

the acceptor (Figure 37).[148] Strong photoluminescence quenching is observed in the polymer blend indicating that photoinduced charge transfer occurs between the two polymers. The power conversion efficiency of these OPV cells approaches 1% after 120 °C postannealing. The authors attributed the improved efficiency to better morphological features of the photoactive layer after thermal annealing.

OPV cells incorporating diimide-based acceptor polymers are among the most efficient among all-polymer solar cells to be reported. The PDI-based polymer acceptor (**P54**, Figure 18) discussed in the n-channel semiconductor section was also used as an acceptor in conjunction with a bis(thienylenevinylene)-substituted polythiophene donor resulting in efficiencies surpassing 1% (Figure 15).[74] More recently, OPVs based on a related donor (a tris-(thienylenevinylene)-substituted polythiophene) and a related acceptor (**P91**) were found, by optimizing the donor: acceptor ratio to exhibit PCEs as high as 1.5% (AM1.5, 100 mW cm^{-2}).[149] Using an alternating PDI-phenylene-vinylene copolymer (**P92**) acceptor and poly(3-phenyl hydrazone thiophene) donor in OPVs, Mikroyannidis et al. obtained a PCE of 2.3% under white-light illumination calibrated to an AM1.5 intensity of 30 mW cm^{-2}, after annealing at 80 °C for 10 min.[150] Very recently, Loo investigated **P58** in combination with P3HT, achieving PCEs approaching 0.6%; they also found that PCEs of

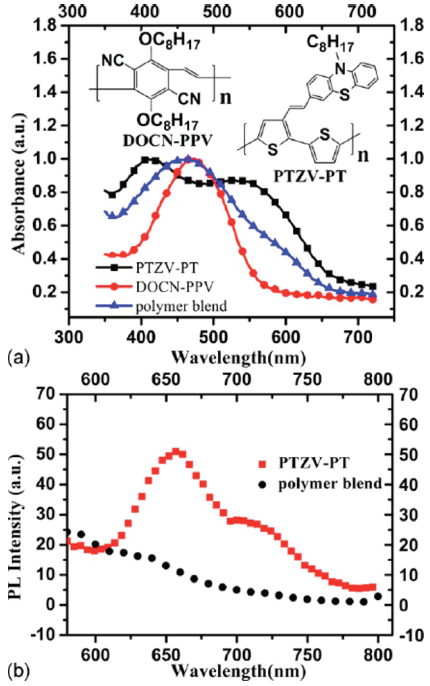

Figure 37. (a) Normalized film absorption spectra of donor PTZV-TV (inset see structure), acceptor **P89**, and the blend. (b) PL spectra of pure PTZV-PT film and polymer blend film. Reprinted with permission from ref 146. Copyright 2010 American Chemical Society.

these blends are more sensitive to the active layer film morphology than are P3HT-$PC_{61}BM$ blends.[151] The ladder polymer **P49** (Figure 17) has also been used to fabricate efficient bilayer cells (PCE = 1.1% at 80 mW cm^{-2} AM1.5) in conjunction with a poly(phenylene vinylene) donor.[152]

Finally, donor−acceptor diblock copolymers in which a polyacrylate chain having pendant perylene diimide (PDI) units (**P93**) serves as the acceptor block have been studied; these materials undergo microscale phase segregation, as single-component active layers in OPV cells. Devices based on such block copolymers with a 4-(diphenylamino)styrene donor block were recently reported to exhibit efficiencies of up to 0.11%,[153] while annealed devices based on **P93** in which the donor block is regioregular poly(3-hexylthiophene) afford a PCE of 0.49%.[154]

Although conjugated polymers exhibit large mobilities and broader optical absorption than fullerenes, power conversion efficiencies of polymer-based OPV cells do not yet rival those of the molecular acceptors. The reason is unclear at present, but an ideal morphology and appropriate electronic coupling with the donor component are issues that warrant further study. In general, the feature size of phase separation in polymer/polymer blend is hundreds of nanometers due to the low entropy of mixing, while in the case of polymer/$PC_{61(71)}BM$ systems, the phase separation length scale is only 10−20 nm. Thus, the donor/acceptor interfacial area in the polymer/fullerenes systems is far larger than that in polymer/polymer systems. Given the fact that typical exciton diffusion lengths in disordered blend layers is approximately 10 nm, the greater phase separation length scale and smaller donor/acceptor interfacial area in the polymer/polymer system is likely responsible for inefficient exciton dissociation and lower PCEs in these systems.[155]

5. Conclusions

In this review several polymeric semiconductors for thin-film transistors and photovoltaic cells were reviewed. It is now clear that during the last 2−3 years impressive results in developing new n-channel polymeric semiconductors were achieved, and the performance difference with the p-channel counterpart has been dramatically reduced. We have shown several examples where modification of the π-conjugated core results in dramatic variation and majority charge carrier from p- to n-channel to ambipolar transport. Importantly from the technology perspective, some of these materials exhibit, as solution processed films, carrier mobilities and I_{on}:I_{off} surpassing those of amorphous Si (> 0.1 cm^2/(V s)). As far as organic photovoltaic cells are concerned, during the past few years OPV cell efficiencies have doubled, now surpassing 8%. These performance were unthinkable only very recently. Thus, polymeric semiconductors are exciting materials and are essential to move these new fields forward toward market applications.

Acknowledgment. Work at Northwestern was supported by AFOSR, ONR, Polyera Corp., BSF, ETRI, and the Northwestern MRSEC.

References

(1) (a) *Handbook of Organic Conductive Molecules and Polymers*; Nalwa, H. S., Ed.; John Wiley & Sons: Chichester, 1997; Vols. *1*−*4*.(b) *Electronic Materials: The Oligomer Approach*; Müllen, K., Wegner, G., Eds.; Wiley-VCH: New York, 1998.

(2) (a) *Organic Electronic Materials: Conjugated Polymers and Low Molecular Weight Organic Solids*; Farchioni, R., Grosso, G., Eds.; Springer: Berlin, 2001.(b) *Electronic Materials: From Silicon to Organics*; Miller, L. S., Mullin, J. B., Eds.;Plenum Press: New York, 1991.

(3) (a) Kelley, T. W.; Baude, P. F.; Gerlach, C.; Ender, D. E.; Muyres, D.; Haase, M. A.; Vogel, D. E.; Theiss, S. D. *Chem. Mater.* **2004**, *16*, 4413. (d) Forrest, S. R. *Nature* **2004**, *428*, 911. (b) Tsutsui, T.; Fujita, K. *Adv. Mater.* **2002**, *14*, 949. (c) Shaw, J. M.; Seidler, P. F. *IBM J. Res. Dev.* **2001**, *45*, 3.

(4) (a) Pingel, P.; Zhu, L.; Park, K. S.; Vogel, J.-O.; Janietz, S.; Kim, E.-G.; Rabe, J. P.; Bredas, J.-L.; Koch, N. *J. Phys. Chem. Lett.* **2010**, *1*, 2037. (b) Chang, H.-C.; Ruden, P. P.; Liang, Y.; Frisbie, C. D. *J. Appl. Phys.* **2010**, *107*, 104502/1. (c) Gutierrez Lezama, I.; Morpurgo, A. F. *Phys. Rev. Lett.* **2009**, *103*, 066803/1. (d) Bredas, J.-L.; Norton, J. E.; Cornil, J.; Coropceanu, V. *Acc. Chem. Res.* **2009**, *42*, 1691. (e) Troisi, A. *Adv. Polym. Sci.* **2010**, *223*, 259. (f) Choi, S. H.; Risko, C.; Ruiz Delgado, M. C.; Kim, B. S.; Bredas, J.-L.; Frisbie, C. D. *J. Am. Chem. Soc.* **2010**, *132*, 4358. (g) Liu, C.; Sirringhaus, H. *Org. Electron.* **2010**, *11*, 558.

(5) (a) Sekitani, T.; Someya, T. *Adv. Mater.* **2010**, *22*, 2228. (b) Ma, H; Yip, H.-L.; Huang, F.; Jen, A. K.-Y. *Adv. Funct. Mater.* **2010**, *20*, 1371. (c) Wu, W.; Liu, Y.; Zhu, D. *Chem. Soc. Rev.* **2010**, *39*, 1489. (d) Ortiz, R. P.; Yan, H.; Facchetti, A.; Marks, T. J. *Materials* **2010**, *3*, 1533. (e) Wen, Y.; Liu, Y. *Adv. Mater.* **2010**, *22*, 1331. (f) Lee, W. H.; Cho, J. H.; Cho, K. *J. Mater. Chem.* **2010**, *20*, 2549. (g) Miozzo, L.; Yassar, A.; Horowitz, G. *J. Mater. Chem.* **2010**, *20*, 2513. (h) Smith, J.; Hamilton, R.; McCulloch, I.; Stingelin-Stutzmann, N.; Heeney, M.; Bradley, D. D. C.; Anthopoulos, T. D. *J. Mater. Chem.* **2010**, *20*, 2562. (i) Singh, M.; Haverinen, H. M.; Dhagat, P.; Jabbour, G. E. *Adv. Mater.* **2010**, *22*, 673. (j) Hoppe, A.; Balster, T.; Muck, T.; Wagner, V. *Org. Electron.* **2009**, 469. (k) Hamilton, R.; Heeney, M.; Anthopoulos, T.; McCulloch, I. *Org. Electron.* **2010**, 393. (l) Kaake, L. G.; Barbara, P. F.; Zhu, X.-Y. *J. Phys. Chem. Lett.* **2010**, *1*, 628. (m) Sirringhaus, H. *Adv. Mater.* **2009**, *21*, 3859. (n) Ortiz, R. P.; Facchetti, A.; Marks, T. J. *Chem. Rev.* **2010**, *110*, 205. (o) Yamashita, Y. *Chem. Lett.* **2009**, *38*, 870. (p) Ohshita, J. *Macromol. Chem. Phys.* **2009**, *210*, 1360. (q) Katz, H. E.; Huang, J. *Annu. Rev. Mater. Res.* **2009**, *39*, 71. (r) Di, C.-A.; Liu, Y.; Yu, G.; Zhu, D. *Acc. Chem. Res.* **2009**, *42*, 1573. (s) Roberts, M. E.; Sokolov, A. N.; Bao, Z. *J. Mater. Chem.* **2009**, *19*, 3351.

(t) DiBenedetto, S. A.; Facchetti, A.; Ratner, M. A.; Marks, T. *J. Adv. Mater.* **2009**, *21*, 1407. (u) Braga, D.; Horowitz, G. *Adv. Mater.* **2009**, *21*, 1473. (v) McCulloch, I.; Heeney, M.; Chabinyc, M. L.; De Longchamp, De.; Kline, R. J.; Colle, M.; Duffy, W.; Fischer, D.; Gundlach, D.; Hamadani, B.; Hamilton, R.; Richter, L.; Salleo, A.; Shkunov, M.; Sparrowe, D.; Tierney, S.; Zhang, W. *Adv. Mater.* **2009**, *21*, 1091. (w) Zhan, Xi.; Barlow, S.; Marder, S. R. *Chem. Commun.* **2009**, 1948. (x) Panzer, M. J.; Frisbie, C. D. *Adv. Mater.* **2008**, *20*, 3177. (zb) de Boer, B.; Facchetti, A. *Polym. Rev.* **2008**, *48*, 423.

(6) (a) Gaudiana, R. *J. Phys. Chem. Lett.* **2010**, *1*, 1288. (b) Giridharagopal, R.; Ginger, D. S. *J. Phys. Chem. Lett.* **2010**, *1*, 1160. (c) Steim, R.; Kogler, F. R.; Brabec, C. J. *J. Mater. Chem.* **2010**, *20*, 2499. (d) Bredas, J.-L.; Durrant, J. R. *Acc. Chem. Res.* **2009**, *42*, 1689. (e) Nelson, J.; Kwiatkowski, J. J.; Kirkpatrick, J.; Frost, J. M. *Acc. Chem. Res.* **2009**, *42*, 1768. (f) Cheng, Y.-J.; Yang, S.-H.; Hsu, C.-S *Chem. Rev.* **2009**, *109*, 5868. (g) Heremans, P.; Cheyns, D.; Rand, B. P. *Acc. Chem. Res.* **2009**, *42*, 1740. (h) Potscavage, W. J., Jr.; Sharma, A.; Kippelen, B. *Acc. Chem. Res.* **2009**, *42*, 1758. (i) Roncali, J. *Acc. Chem. Res.* **2009**, *42*, 1719. (j) Chen, J.; Cao, Y. *Acc. Chem. Res.* **2009**, *42*, 1709. (k) Dennler, G.; Scharber, M. C.; Brabec, C. *Adv. Mater.* **2009**, *21*, 1323. (l) Pagliaro, M.; Ciriminna, R.; Palmisano, G. *ChemSusChem* **2008**, *1*, 880.

(7) (a) *Organic Semiconductors and Devices*; Malliaras, G., Ed.; John Wiley & Sons: Hoboken, 2003. (b) Karl, N. *Synth. Met.* **2003**, *133*−*134*, 649.

(8) (a) Sirringhaus, H. *Nat. Mater.* **2003**, *2*, 641. (b) Pron, A.; Rannou Progr., P. *Polym. Sci* **2002**, *27*, 135. (c) Cacialli, F. *Philos. Trans. R. Soc. London, Ser. A* **2000**, *358*, 173. (d) Kowalsky, W.; Becker, E; Benstem, T.; Johannes, H.-H.; Metzdorf, D.; Neuner, H.; Schobel, J. *Adv. Solid State Phys.* **2000**, *40*, 795. (e) Horowitz, G. *Adv. Mater.* **1990**, *2*, 287.

(9) (a) Katz, H. E. *Chem. Mater.* **2004**, *16*, 4748. (b) Allard, S.; Forster, M.; Souharce, B.; Thiem, H.; Scherf, U. *Angew. Chem., Int. Ed.* **2008**, *47*, 4070.

(10) Hamilton, R.; Bailey, C.; Duffy, W.; Heeney, M.; Shkunov, M.; Sparrowe, D.; Tierney, S.; McCulloch, I.; Kline, R. J.; DeLongchamp, D. M.; Chabinyc, M. *Proc. SPIE—Int. Soc. Opt. Eng.* **2006**, *6336*, 158.

(11) (a) *Organic Electronics: Materials,Manu facturing, and Applications*; Klauk, H., Ed.; Wiley-VCH: Weinheim, Germany, 2006.(b) *Flexible flat panel display*; Crawford, G. P., Ed.; Wiley: New York, 2005.(c) *Printed organic and molecular electronics*; Gamota, D., Brazis, P., Kalyanasumdaram, K., Zhang, J., Eds.; Kluwer Academic: Boston, 2004.

(12) Pron, A.; Rannou, P. *Prog. Polym. Sci.* **2002**, *27*, 135.

(13) Perepichka, I. F.; Perepichka, D. F.; Meng, H.; Wudl, F. *Adv. Mater.* **2005**, *17*, 2281.

(14) Kline, R. J.; McGehee, M. D.; Kadnikova, E. N.; Liu, J.; Frechet, J. M. J.; Toney, M. F. *Macromolecules* **2005**, *38*, 3312.

(15) Zen, A.; Saphiannikova, M.; Neher, D.; Grenzer, J.; Grigorian, S.; Pietsch, U.; Asawapirom, U.; Janietz, S.; Scherf, U.; Lieberwirth, I.; Wegner, G. *Macromolecules* **2006**, *39*, 2162.

(16) Zhang, R.; Li, B.; Iovu, M. C.; Jeffries-EL, M.; Sauve, G.; Cooper, J.; Jia, S.; Tristram-Nagle, S.; Smilgies, D. M.; Lambeth, D. N.; McCullough, R. D.; Kowalewski, T. *J. Am. Chem. Soc.* **2006**, *128*, 3480.

(17) Chang, J.-F.; Sun, B.; Breiby, D. W.; Nielsen, M. M.; Soelling, T. I.; Giles, M.; McCulloch, I.; Sirringhaus, H. *Chem. Mater.* **2004**, *16*, 4772.

(18) Majewski, L. A.; Kingsley, J. W.; Balocco, C.; Song, A. M. *Appl. Phys. Lett.* **2006**, *88*, 222108/1.

(19) Surin, M.; Leclere, Ph.; Lazzaroni, R.; Yuen, J. D.; Wang, G.; Moses, D.; Heeger, A. J.; Cho, S.; Lee, K. *J. Appl. Phys.* **2006**, *100*, 033712.

(20) Jia, H.; Gowrisanker, S.; Pant, G. K.; Wallace, R. M.; Gnade, B. E. *J. Vac. Sci. Technol., A* **2006**, *24*, 1228.

(21) Kim, D. H.; Jang, Y.; Park, Y. D.; Cho, K. *J. Phys. Chem. B* **2006**, *110*, 15763.

(22) Hoshino, S.; Yoshida, M.; Uemura, S.; Kodzasa, T.; Takada, N.; Kamata, T.; Yase, K. *J. Appl. Phys.* **2004**, *95*, 5088–5093.

(23) Park, Y. D.; Kim, D. H.; Jang, Y.; Cho, J. H.; Hwang, M.; Lee, H. S.; Lim, J. A.; Cho, K. *Org. Electron.* **2006**, *7*, 514.

(24) Bao, Z.; Feng, Y.; Dodabalapur, A.; Raju, V. R.; Lovinger, A. J. *Chem. Mater.* **1997**, *9*, 1299.

(25) Ong, B. S.; Wu, Y.; Liu, P.; Gardner, S. *J. Am. Chem. Soc.* **2004**, *126*, 3378.

(26) Chabinyc, M. L.; Endicott, F.; Vogt, B. D.; DeLongchamp, D. M.; Lin, E. K.; Wu, Y.; Liu, P.; Ong, B. S. *Appl. Phys. Lett.* **2006**, *88*, 113514/1.

(27) Heeney, M.; Bailey, C.; Genevicius, K.; Shkunov, M.; Sparrowe, D.; Tierney, S.; McCulloch, I. *J. Am. Chem. Soc.* **2005**, *127*, 1078.

(28) McCulloch, I.; Heeney, M.; Bailey, C.; Genevicius, K.; MacDonald, I.; Shkunov, M.; Sparrowe, D.; Tierney, S.; Wagner, R.; Zhang, W.; Chabinyc, M. L.; Kline, R. J.; McGehee, M. D.; Toney, M. F. *Nat. Mater.* **2006**, *5*, 328.

(29) DeLongchamp, D. M.; Kline, R. J.; Lin, E. K.; Fischer, D. A.; Richter, L. J.; Lucas, L. A.; Heeney, M.; McCulloch, I.; Northrup, J. E. *Adv. Mater.* **2007**, *19*, 833.

(30) Chua, L.-L.; Ho, P. K. H.; Sirringhaus, H.; Friend, R. H. *Adv. Mater.* **2004**, *16*, 1609–1615.

(31) Yan, H.; Yoon, M.-H; Facchetti, A.; Marks, T. J. *Appl. Phys. Lett.* **2005**, *87*, 183501.

(32) (a) Fielke, D.; Huebler, A. C.; Hahn, U.; Brandt, N.; Bartzsch, M.; Fuegmann, U.; Fischer, T.; Veres, J.; Ogier, S. *Appl. Phys. Lett.* **2005**, *87*, 123508/1. (b) Veres, J.; Ogier, S. D.; Leeming, S. W.; Cupertino, D. C.; Khaffaf, S. M. *Adv. Funct. Mater.* **2003**, *13*, 199.

(33) Li, Y.; Wu, Y.; Ong, B. S. *Macromolecules* **2006**, *39*, 6521.

(34) Drolet, N.; Morin, J.-F.; Leclerc, N.; Wakim, S.; Tao, Y.; Leclerc, M. *Adv. Funct. Mater.* **2005**, *15*, 1671.

(35) (a) Ogawa, K.; Rasmussen, S. C. *J. Org. Chem.* **2003**, *68*, 2921. (b) Ogawa, K.; Stafford, J. A.; Rothstein, S. D.; Tallman, D. E.; Rasmussen, S. C. *Synth. Met.* **2005**, *152*, 137.

(36) (a) Ogawa, K.; Rasmussen, S. C. *Macromolecules* **2006**, *39*, 1771. (b) Koeckelberghs, G.; Samyn, C. *Macromolecules* **2005**, *38*, 4545.

(37) Liu, J.; Zhang, R.; Sauve, G.; Kowalewski, T.; McCullough, R. D. *J. Am. Chem. Soc.* **2008**, *130*, 13167.

(38) (a) Yamamoto, T.; Kokubo, H.; Kobashi, M.; Sakai, Y. *J. Mater. Chem.* **2004**, *16*, 4616. (b) Yamamoto, T.; Arai, M.; Kokubo, H.; Sasaki, S. *Macromolecules* **2003**, *36*, 7986. (c) Li, W.; Katz, H.; Lovinger, A.; Laquindanum, J. *Chem. Mater.* **1999**, *11*, 458.

(39) Liu, J.; Zhang, R.; Osaka, I.; Mishra, S.; Javier, A. E.; Smilgies, D.; Kowalewski, T.; McCullough, R. D. *Adv. Funct. Mater.* **2009**, *19*, 3427.

(40) Fong, H. H.; Pozdin, V. A.; Amassian, A.; Malliaras, G. G.; Smilgies, D.-M.; He, M.; Gasper, S.; Zhang, F.; Sorensen, M. *J. Am. Chem. Soc.* **2008**, *130*, 13202. (b) He, M.; Li, J.; Sorensen, M. L.; Zhang, F.; Hancock, R. R.; Fong, H. H.; Pozdin, V. A.; Smilgies, D.-M.; Malliaras, G. G. *J. Am. Chem. Soc.* **2009**, *131*, 11930.

(41) He, M.; Li, J.; Tandia, A.; Sorensen, M.; Zhang, F.; Fong, H. H.; Pozdin, V. A.; Smilgies, D.; Malliaras, G. G. *Chem. Mater.* **2010**, *22*, 2770.

(42) Li, J.; Qin, F.; Li, C. M.; Bao, Q.; Chan-Park, M. B.; Zhang, W.; Qin, J.; Ong, B. S. *Chem. Mater.* **2008**, *20*, 2057.

(43) Rieger, R.; Beckmann, D.; Pisula, W.; Steffen, W.; Kastler, M.; Mullen, K. *Adv. Mater.* **2010**, *22*, 83.

(44) Prosa, T. J.; Winokur, M. J.; Moulton, J.; Smith, P.; Heeger, A. J. *Macromolecules* **1992**, *25*, 4364.

(45) Nakayama, J.; Fujimiri, T. *Heterocycles* **1991**, *32*, 991.

(46) (a) Fu, Y.; Cheng, H.; Elsenbaumer, R. L. *Chem. Mater.* **1997**, *9*, 1720. (b) Elandaloussi, E. H.; Frère, P.; Richomme, P.; Orduna, J.; Garin, J.; Roncali, J. *J. Am. Chem. Soc.* **1997**, *119*, 10774.

(47) (a) Payne, M.; Parkin, S.; Anthony, J.; Kuo, C.; Jackson, T. *J. Am. Chem. Soc.* **2005**, *127*, 4986. (b) Stingelin-Stutzmann, N.; Smits, E.; Wondergem, H.; Tanase, C.; Blom, P.; Smith, P.; de Leeuw, D. M. *Nat. Mater.* **2005**, *4*, 601. (c) Mathijssen, S. G. J.; Cölle, M.; Gomes, H.; Smits, E. C. P.; de Boer, B.; McCulloch, I.; Bobbert, P. A.; de Leeuw, D. M. *Adv. Mater.* **2007**, *19*, 2785. (d) Mathijssen, S. G. J.; Kemerink, M.; Sharma, A.; Colle, M.; Bobbert, P. A.; Janssen, R. A. J.; de Leeuw, D. M. *Adv. Mater.* **2008**, *20*, 975. (e) Street, R. A.; Chabinyc, M. L.; Endicott, F.; Ong, B. *J. Appl. Phys.* **2006**, *100*, 114518. (f) Street, R. A.; Salleo, A.; Chabinyc, M. *Phys. Rev. B* **2003**, *68*, 085316. (g) Salleo, A.; Street, R. A. *Phys. Rev. B* **2004**, *70*, 235324. (h) Salleo, A.; Endicott, F.; Street, R. A. *Appl. Phys. Lett.* **2005**, *86*, 263505.

(48) Tsukada, T. In *Technology and Applications of Amorphous Silicon*; Street, R. A., Ed.; Springer-Verlag: Heidelberg, 2000; Vol. *37*, p 49.

(49) Kim, D. H.; Lee, B.; Moon, H.; Kang, H. M.; Jeong, E. J.; Park, J.; Han, K.; Lee, S.; Yoo, B. W.; Koo, B. W.; Kim, J. Y.; Lee, W. H.; Cho, K.; Becerril, H. A.; Bao, Z. *J. Am. Chem. Soc.* **2009**, *131*, 6124.

(50) McCulloch, I.; Heeney, M.; Bailey, C.; Genevicius, K.; Macdonald, I.; Shkunov, M.; Sparrowe, D.; Tierney, S.; Wagner, R.; Zhang, W.; Chabinyc, M. L.; Kline, R. J.; McGehee, M. D.; Toney, M. F. *Nat. Mater.* **2006**, *5*, 328.

(51) (a) Yamamoto, T.; Arai, M.; Kokudo, H.; Sasaki, S. *Macromolecules* **2003**, *36*, 7986. (b) Yamamoto, T.; Kokudo, H.; Kobashi, M.; Sakai, Y. *Chem. Mater.* **2004**, *16*, 4616. (c) Kokudo, H.; Sato, T.; Yamamoto, T. *Macromolecules* **2006**, *39*, 3959.

(52) Osaka, I.; Zhang, R.; Sauve, G.; Smilgies, D; Kowalewski, T.; McCullough, R. D. *J. Am. Chem. Soc.* **2009**, *131*, 2521.

(53) (a) Jenekhe, S. A.; Osaheni, J. A. *Science* **1994**, *265*, 765. (b) Osaheni, J. A.; Jenekhe, S. A. *J. Am. Chem. Soc.* **1995**, *117*, 7389. (c) So, Y.-H.; Zaleski, J. M.; Murlick, C.; Ellaboudy, A. *Macromolecules* **1996**, *29*, 2783. (d) Mike, J. F.; Makowski, A. J.; Jeffries-EL, M. *Org. Lett.* **2008**, *10*, 4915.

(54) (a) Wolfe, J. F.; Loo, B. H.; Arnold, F. E. *Macromolecules* **1981**, *14*, 915. (b) Choe, E. W.; Kim, S. N. *Macromolecules* **1981**, *14*, 920. (c) Roberts, M. F.; Jenekhe, S. A. *Chem. Mater.* **1993**, *5*, 1744. (d) Osaheni, J. A.; Jenekhe, S. A. *Chem. Mater.* **1995**, *7*, 672. (e) Osaheni, J. A.; Jenekhe, S. A. *Macromolecules* **1993**, *26*, 4726. (f) Alam, M. M.; Jenekhe, S. A. *Chem. Mater.* **2002**, *14*, 4775. (g) Jenekhe, S. A.; Osaheni, J. A.; Meth, J. S.; Vanherzeele, H. *Chem. Mater.* **1992**, *4*, 683. (h) Osaheni, J. A.; Jenekhe, S. A. *Chem. Mater.* **1992**, *4*, 1282. (i) Dotrong, M.; Mehta, R.; Balchin, G. A.; Tomlinson, R. C.; Sinsky, M.; Lee, C. Y. C.; Evers, R. C. *J. Polym. Sci., Part A: Polym. Chem.* **1993**, *31*, 723.

(55) (a) Babel, A.; Jenekhe, S. A. *J. Phys. Chem. B* **2002**, *106*, 6129. (b) Babel, A.; Jenekhe, S. A. *J. Am. Chem. Soc.* **2003**, *125*, 13656.

(56) (a) Pang, H.; Vilela, F.; Skabara, P. J.; McDouall, J. J. W.; Crouch, D. J.; Anthopoulos, T. D.; Bradley, D. D. C.; de Leeuw, D.; Horton, P. N.; Hursthouse, M. B. *Adv. Mater.* **2007**, *19*, 4438. (b) Mamada, M.; Nishida, J.-I.; Tokito, S.; Yamashita, Y. *Chem. Lett.* **2008**, *37*, 766.

(57) Zhang, W.; Smith, J.; Hamilton, R.; Heeney, M.; Kirkpatrick, J.; Song, K.; Watkins, S. E.; Anthopoulos, T.; McCulloch, I. *J. Am. Chem. Soc.* **2009**, *131*, 10814.

(58) Zhang, W.; Smith, J.; Watkins, S. W.; Gysel, R.; McGehee, M; Salleo, A.; Kirkpatrick, J.; Ashraf, S.; Anthopoulos, T.; Heeney, M.; McCulloch, I. *J. Am. Chem. Soc.* **2010**, *132*, 11437.

(59) Mathijssen, S. G. J.; Coelle, M.; Gomes, H.; Smits, E. C. P.; de Boer, B.; McCulloch, I.; Bobbert, P. A.; de Leeuw, D. M. *Adv. Mater.* **2007**, *19*, 2785.

(60) (a) Usta, H.; Lu, G.; Facchetti, A.; Marks, T. J. *J. Am. Chem. Soc.* **2006**, *128*, 9034–9035. (b) Usta, H.; Facchetti, A.; Marks, T. J. *J. Am. Chem. Soc.* **2008**, *130*, 8580–8581.

(61) Beaujuge, P. M.; Pisula, W.; Tsao, H. N.; Ellinger, S.; Mullen, K.; Reynolds, J. R. *J. Am. Chem. Soc.* **2009**, *131*, 7514–7515.

(62) Mondal, R.; Miyaki, N.; Becerril, H. A.; Norton, J. E.; Parmer, J.; Mayer, A. C.; Tang, M. L.; Bredas, J. -L; McGehee, M. D.; Bao, Z. *Chem. Mater.* **2009**, *21*, 3618.

(63) (a) Takimiya, K.; Ebata, H.; Sakamoto, K.; Izawa, T.; Otsubo, T.; Kunugi, Y. *J. Am. Chem. Soc.* **2006**, *128*, 12604. (b) Ebata, H.; Izawa, T.; Miyazaki, E.; Takimiya, K.; Ikeda, M.; Kuwabara, H.; Yui, T. *J. Am. Chem. Soc.* **2007**, *129*, 15732.

(64) Osaka, I.; Abe, T.; Shinamura, S.; Miyazaki, E.; Takimiya, K. *J. Am. Chem. Soc.* **2010**, *132*, 5000.

(65) Shinamura, S.; Miyazaki, E.; Takimiya, K. *J. Org. Chem.* **2010**, *75*, 1228.

(66) Yang, C.; Cho, S.; Chiechi, R. C.; Walker, W.; Coates, N. E.; Moses, D.; Heeger, A. J.; Wudl, F. *J. Am. Chem. Soc.* **2008**, *130*, 16524.

(67) Guo, X.; Kim, F. S.; Jenekhe, S. A.; Watson, M. D. *J. Am. Chem. Soc.* **2009**, *131*, 7206–7207.

(68) (a) Bleiholder, C.; Gleiter, R.; Werz, D. B.; Koeppel, H. *Inorg. Chem.* **2007**, *46*, 2249. (b) Pomerantz, M. *Tetrahedron Lett.* **2003**, *44*, 1563. (c) Irvin, J. A.; Schwendeman, I.; Lee, Y.; Abboud, K. A.; Reynolds, J. R. *J. Polym. Sci., Part A: Polym. Chem.* **2001**, *39*, 2164. (d) Cloutier, R.; Leclerc, M. *J. Chem. Soc., Chem. Commun.* **1991**, 1194. (e) Vangheluwe, M.; Verbiest, T.; Koeckelberghs, G. *Macromolecules* **2008**, *41*, 1041.

(69) (a) Thompson, B. C.; Kim, Y. G.; McCarley, T. D.; Reynolds, J. R. *J. Am. Chem. Soc.* **2006**, *128*, 12714. (b) Roncali, J. *Chem. Rev.* **1997**, *97*, 173.

(70) (a) Yoon, M.-Y.; Kim, C., S.; Facchetti, A.; Marks, T. J. *J. Am. Chem. Soc.* **2006**, *128*, 12851. (b) Chua, L. L.; Zaumseil, J.; Chang, J. F.; Ou, E. C. W.; Ho, P. K. H.; Sirringhaus, H.; Friend, R. H. *Nature* **2005**, *434*, 194.

(71) Babel, A.; Jenekhe, S. A. *J. Am. Chem. Soc.* **2003**, *125*, 13656.

(72) Briseno, A. L.; Mannsfeld, S. C. B.; Shamberger, P. J.; Ohuchi, F. S.; Bao, Z.; Jenekhe, A.; Samson; Xia, Y. *Chem. Mater.* **2008**, *20*(14), 4712.

(73) Usta, H.; Facchetti, A.; Marks, T. J. *J. Am. Chem. Soc.* **2008**, *130*, 8580.

(74) Letizia, J.; Salata, M.; Tribout, C.; Facchetti, A.; Ratner, M. A.; Marks, T. J. *J. Am. Chem. Soc.* **2008**, *130*, 9679.

(75) Zhan, X.; Tan, Z.; Domercq, B.; An, Z.; Zhang, X.; Barlow, S.; Li, Y.; Zhu, D.; Kippelen, B.; Marder, S. R. *J. Am. Chem. Soc.* **2007**, *129*, 7246.

(76) Zhan, X.; Tan, Z.; Zhou, E.; Li, Y.; Misra, R.; Grant, A.; Domercq, B.; Zhang, X.; An, Z.; Zhang, X.; Barlow, S.; Kippelen, B.; Marder, S. R. *J. Mater. Chem.* **2009**, *19*, 5794.

(77) Hüttner, S.; Sommer, M.; Thelakkat, M. *Appl. Phys. Lett.* **2008**, *92*, 093302.

(78) Chen, Z.; Zheng, Y.; Yan, H.; Facchetti, A. *J. Am. Chem. Soc.* **2009**, *131*, 8.

(79) Facchetti, A. Presented at the 9th International Symposium on Functional π-Electron Systems, Atlanta, GA, U.S.A, 2010.

(80) Yan, H.; Chen, Z.; Zheng, Y.; Newman, C. E.; Quin, J.; Dolz, F; Kastler, M.; Facchetti, A. *Nature* **2009**, *457*, 679.

(81) Baeg, K.-J.; Khim, D.; Kim, D.-Y.; Jung, S.-W.; Koo, J. B.; You, I.-K.; Yan, H.; Facchetti, A.; Noh, Y.-Y. *J. Polym. Sci., Part B: Polym. Phys.* **2011**, *49*, 62–67.

(82) (a) DeLongchamp, D. M.; Kline, R. J.; Lin, E. K.; Fischer, D. A.; Richter, L. J.; Lucas, L. A.; Heeney, M.; McCulloch, I.; Northrup, J. E. *Adv. Mater.* **2007**, *19*, 833. (b) Sirringhaus, H.; Brown, P. J.; Friend, R. H.; Nielsen, M. M.; Bechgaard, K.; Langeveld-Voss, B. M. W.; Spiering, A. J. H.; Janssen, R. A. J.; Meijer, E. W.; Herwig, P.; de Leeuw, D. M. *Nature* **1999**, *401*, 685. (c) Kline, R. J.; McGehee, M. D.; Toney, M. F. *Nat. Mater.* **2006**, *5*, 222. (d) Kim, D. H.; Park, Y. D.; Jang, Y.; Yang, H.; Kim, Y. H.; Han, J. I.; Moon, D. G.; Park, S.; Chang, T.; Chang, C.; Joo, M.; Ryu, C. Y.; Cho, K. *Adv. Funct. Mater.* **2005**, *15*, 77. (e) Street, R. A.; Northrup, J. E.; Salleo, A. *Phys. Rev. B* **2005**, *71*, 165202. (f) Tsao, H. N.; Cho, D.; Andreasen, J. W.; Rouhanipour, A.; Breiby, D. W.; Pisula, W.; Müllen, K. *Adv. Mater.* **2009**, *21*, 209. (g) Yang, H.; Shin, T. J.; Yang, L.; Cho, K.; Ryu, C. Y.; Bao, Z. *Adv. Funct. Mater.* **2005**, *15*, 671.

(83) (a) Street, R. A.; Northrup, J. E.; Salleo, A. *Phys. Rev. B* **2005**, *71*, 165202. (b) Kline, R. J.; DeLongchamp, D. M.; Fischer, D. A.; Lin, E. K.; Heeney, M.; McCulloch, I.; Toney, M. F. *Appl. Phys. Lett.* **2007**, *90*, 062117. (c) Salleo, A. *Mater. Today* **2007**, *10*, 38.

(84) Rivnay, J.; Toney, M. F.; Zheng, Y.; Kauvar, I. V.; Chen, Z.; Wagner, V.; Facchetti, A.; Salleo, A. *Adv. Mater.* **2010**, *22*, 4359–4363.

(85) Steyrleuthner, R.; Schubert, M.; Jaiser, F.; Blakesley, J. C.; Chen, Z.; Facchetti, A.; Neher, D. *Adv. Mater.* **2010**, *22*, 2799.

(86) (a) Mandoc, M. M.; de Boer, B.; Blom, P. W. M. *Phys. Rev. B* **2006**, *73*, 155205. (b) Steyrleuthner, R.; Bange, S.; Neher, D. *J. Appl. Phys.* **2009**, *105*, 8.

(87) (a) Shkunov, M.; Simms, R.; Heeney, M.; Tierney, S.; McCulloch, I. *Adv. Mater.* **2005**, *17*, 2608.(b) Kang, S.-M.; Leblebici, Y. *CMOS Digital Integrated Circuits: Analysis and Design*; McGraw-Hill, New York, 1996.

(88) (a) Anthopoulos, T. D.; de Leeuw, D. M.; Cantatore, E.; Setayesh, S.; Meijer, E. J.; Tanase, C.; Hummelen, J. C.; Blom, P. W. M. *Appl. Phys. Lett.* **2004**, *85*, 4205. (b) Anthopoulos, T. D.; de Leeuw, D. M.; Cantatore, E.; van't Hof, P.; Alma, J.; Hummelen, J. C. *J. Appl. Phys.* **2005**, *98*, 6. (c) Anthopoulos, T. D.; Setayesh, S.; Smits, E.; Cölle, M.; Cantatore, E.; de Boer, B.; Blom, P. W. M.; de Leeuw, D. M. *Adv. Mater.* **2006**, *18*, 1900.

(89) (a) Capelli, R.; Toffanin, S.; Generali, G.; Usta, H.; Facchetti, A.; Muccini, M. *Nat. Mater.* **2010**, *9*, 496. (b) Swensen, J. S.; Soci, C.; Heeger, A. J. *Appl. Phys. Lett.* **2005**, *87*, 3. (c) Generali, G.; Capelli, R.; Toffanin, S.; Facchetti, A.; Muccini, M. *Microelectron. Reliab.* **2010**, *50*, 1861. (d) Zaumseil, J.; Friend, R. H.; Sirringhaus, H. *Nat. Mater.* **2006**, *5*, 69. (e) Muccini, M. *Nat. Mater.* **2006**, *5*, 605.

(90) Chen, Z.; Lemke, H.; Albert-Seifried, S.; Caironi, M.; Nielsen, M. M.; Heeney, M.; Zhang, W.; McCulloch, I.; Sirringhaus, H. *Adv. Mater.* **2010**, *22*, 2371.

(91) (a) Heeney, M.; Zhang, W.; Crouch, D. J.; Chabinyc, M. L.; Gordeyev, S.; Hamilton, R.; Higgins, S. J.; McCulloch, I.; Skabara, P. J.; Sparrowe, D.; Tierney, S. *Chem. Commun.* **2007**, 5061. (b) Oyaizu, K.; Iwasaki, T.; Tsukahara, Y.; Tsuchida, E. *Macromolecules* **2004**, *37*, 1257.

(92) Meijer, E. J.; De Leeuw, D. M.; Setayesh, S.; Van Veenendaal, E.; Huisman, B. H.; Blom, P. W. M.; Hummelen, J. C; Scherf, U.; Klapwijk, T. M. *Nat. Mater.* **2003**, *2*, 678.

(93) Kim, F. S.; Guo, X.; Watson, M. D.; Jenekhe, S. A. *Adv. Mater.* **2010**, *22*, 478.

(94) Burgi, L.; Turbiez, M.; Pfeiffer, R.; Bienewald, F.; Kirner, H.; Winnewisser, C. *Adv. Mater.* **2009**, *20*, 2217.

(95) Bijleveld, J. C.; Zoombelt, A. P.; Mathijssen, S. G. J.; Wienk, M. M.; Turbiez, M.; de Leeuw, D. M.; Janssen, R. A. J. *J. Am. Chem. Soc.* **2009**, *131*, 16616.

(96) Steckler, T. T.; Zhang, Z.; Hwang, J.; Honeyager, R.; Ohira, S.; Zhang, X.; Grant, A.; Ellinger, S.; Odom, S. A.; Sweat, D.; Tanner, D. B.; Rinzler, A. G.; Barlow, S.; Bredas, J.-L.; Kippelen, B.; Marder, S. R.; Reynolds, J. R. *J. Am. Chem. Soc.* **2009**, *131*, 2824.

(97) Szendrei, K.; Jarzab, D.; Chen, Z.; Facchetti, A.; Loi, M. A. *J. Mater. Chem.* **2010**, *20*, 1317.

(98) (a) Tang, C. W. *Appl. Phys. Lett.* **1986**, *48*, 183. (b) Kim, J. Y.; Lee, K.; Coates, N. E.; Moses, D.; Nguyen, T.-Q.; Dante, M.; Heeger, A. J. *Science* **2007**, *317*, 222.

(99) www.solardaily.com/reports/Solarmer_Energy_Breaks_Psychological_Barrier_999.html (accessed August, 2010).

(100) (a) Yu, G.; Gao, J.; Hummelen, J. C.; Wudl, F.; Heeger, A. J. *Science* **1995**, *270*, 1789. (b) Gunes, S.; Neugebauer, H. S.; Sariciftci, N. S. *Chem. Rev.* **2007**, *107*, 1324. (c) Coakley, K.; McGehee, M. D. *Chem. Mater.* **2004**, *16*, 4533. (d) Li, C.; Liu, M.; Pschirer, N. G.; Baumgarten, M.; Muellen, K. *Chem. Rev.* **2010**, *110*, 6817. (e) Silvestri, F.; Marrocchi, A. *Int. J. Mol. Sci.* **2010**, *11*, 1471.

(101) (a) Brabec, C. J.; Sariciftci, N. S.; Hummelen, J. C. *Adv. Funct. Mater.* **2001**, *11*, 15. (b) Thompson, B. C.; Frechet, J. M. J. *Angew. Chem., Int. Ed.* **2008**, *47*, 58.

(102) Li, Y.; Zou, Y. *Adv. Mater.* **2008**, *20*, 2952.

(103) (a) Wang, L.; Liu, Y.; Jiang, X.; Qin, D.; Cao, Y. *J. Phys. Chem. C* **2007**, *111*, 9538. (b) Hoppe, H.; Sariciftci, N. S. *J. Mater. Chem.* **2006**, *16*, 45. (c) Zheng, L.; Zhou, Q.; Deng, X.; Yuan, M.; Yu, G.; Cao, Y. *J. Phys. Chem. B* **2004**, *108*, 11921. (d) Shaheen, S.; Brabec, C. J.; Sariciftci, N. S.; Padinger, F.; Fromherz, T.; Hummelen, J. C. *Appl. Phys. Lett.* **2001**, *78*, 841.

(104) (a) Zhao, G.; He, Y.; Li, Y. *Adv. Mater.* **2010**, *22*, 0. (b) He, Y.; Chen, H.-Y.; Hou, J.; Li, Y. *J. Am. Chem. Soc.* **2010**, *132*, 1377.

(105) (a) Kim, J. Y.; Lee, K.; Coates, N. E.; Moses, D.; Nguyen, T.-Q.; Dante, M.; Heeger, A. J. *Science* **2007**, *317*, 222. (b) Yu, G.; Gao, J.; Hummelen, J. C.; Wudl, F.; Heeger, A. J. *Science* **1995**, *270*, 1789. (c) Gunes, S.; Neugebauer, H. S.; Sariciftci, N. S. *Chem. Rev.* **2007**, *107*, 1324. (d) Coakley, K.; McGehee, M. D. *Chem. Mater.* **2004**, *16*, 4533–4542. (e) Brabec, C. J.; Sariciftci, N. S.; Hummelen, J. C. *Adv. Funct. Mater.* **2001**, *11*, 15. (f) Thompson, B. C.; Frechet, J. M. J. *Angew. Chem., Int. Ed.* **2008**, *47*, 58. (g) Li, Y.; Zou, Y. *Adv. Mater.* **2008**, *20*, 2952.

(106) Yan, H.; Lee, P.; Graham, A.; Armstrong, N. A.; Evmenenko, G. A.; Dutta, P.; Marks, T. J. *J. Am. Chem. Soc.* **2005**, *127*, 3172.

(107) Hains, A. W.; Marks, T. J. *Appl. Phys. Lett.* **2008**, *92*, 023504.

(108) Chen, L.-M.; Hong, Z.; Li, G.; Yang *Adv. Mater.* **2009**, *21*, 1434.

(109) Irwin, M. D.; Buchholz, D. B.; Hains, A. W.; Chang, R. P. H.; Marks, T. J. *Proc. Natl. Acad. Sci. U.S.A.* **2008**, *105*, 2783.

(110) Beaujuge, P. M.; Amb, C. M.; Reynolds, J. R. Spectral engineering in pi-conjugated polymers with intramolecular donor-acceptor interactions. *Acc. Chem. Res.* **2010**, *43*(11), 1396–1407.

(111) (a) Muhlbacher, D.; Scharber, M.; Morana, M.; Zhu, Z.; Waller, D.; Gaudiana, R.; Brabec, C. *Adv. Mater.* **2006**, *18*, 2884. (b) Peet, J.; Kim, J. Y.; Coates, N. E.; Ma, W. L.; Moses, D.; Heeger, A. J.; Bazan, G. C. *Nat. Mater.* **2007**, *6*, 497. (c) Lee, J. K.; Ma, W. L.; Brabec, C. J.; Yuen, J.; Moon, J. S.; Kim, J. Y.; Lee, K.; Bazan, G. C.; Heeger, A. J. *J. Am. Chem. Soc.* **2008**, *130*, 3619.

(112) Hou, J.; Chen, H. Y.; Zhang, S.; Li, G.; Yang, Y. *J. Am. Chem. Soc.* **2008**, *130*, 16144.
(113) Boudreault, P. L. T.; Michaud, A.; Leclerc, M. *Macromol. Rapid Commun.* **2007**, *28*, 2176.
(114) Wang, E.; Wang, L.; Lan, L.; Luo, C.; Zhuang, W.; Peng, J.; Cao, Y. *Appl. Phys. Lett.* **2008**, *92*, 033307.
(115) Wang, J.-Y.; Hau, S. K.; Yip, H.-L.; Davies, J. A.; Chen, K.-S.; Zhang, Y.; Sun, Y.; Jen, A. K.-Y. *Chem. Mater.* **2010**, DOI: 10.1021/cm1020228.
(116) (a) Zhang, Q. T.; Tour, J. M. *J. Am. Chem. Soc.* **1997**, *119*, 5065. (b) Zhang, Q. T.; Tour, J. M. *J. Am. Chem. Soc.* **1998**, *120*, 5355. (c) Pomerantz, M. *Synth. Met.* **2003**, *135*−*136*, 257. (d) Pomerantz, M. *Tetrahedron Lett.* **2003**, *44*, 1563. (e) Nielsen, C.; Bjornholm, T. *Org. Lett.* **2004**, *6*, 3381.
(117) Zou, Y.; Najari, A.; Berrouard, P.; Beaupre', S.; Badrou, R. A.; Tao, Y.; Leclerc, M. *J. Am. Chem. Soc.* **2010**, *132*, 5330.
(118) (a) Pandey, A. K.; Nunzi, J. M.; Ratier, B.; Moliton, A. *Phys. Lett. A* **2008**, *372*, 1333. (b) Gupta, D.; Bag, M.; Narayan, K. S. *Appl. Phys. Lett.* **2008**, *93*, 163301.
(119) Zhang, G.; Fu, Y.; Zhang, Q.; Xie, Z *Chem. Commun.* **2010**, *46*, 4997.
(120) Piliego, C.; Holcombe, T. W.; Douglas, J. D.; Woo, C. H.; Beaujuge, P. M.; Frechet, J. M. J. *J. Am. Chem. Soc.* **2010**, *132*, 7595.
(121) Peet, J.; Cho, N. S.; Lee, S. K.; Bazan, G. C. *Macromolecules* **2008**, *41*, 8655.
(122) Hou, J.; Park, M. H.; Zhang, S.; Yao, Y.; Chen, L. M.; Li, J. H.; Yang, Y. *Macromolecules* **2008**, *41*, 6012.
(123) Liang, Y.; Wu, Y.; Feng, D.; Tsai, S. T.; Son, H. J.; Li, G.; Yu, L. *J. Am. Chem. Soc.* **2009**, *131*, 56.
(124) Liang, Y.; Xu, Z.; Xia, J.; Tsai, S.-T.; Wu, Y.; Li, G.; Ray, C.; Yu, L. *Adv. Mater.* **2010**, *22*, E135.
(125) (a) Burgi, L.; Turbiez, M.; Pfeiffer, R.; Bienewald, F.; Kirner, H.-J.; Winnewisser, C. *Adv. Mater.* **2008**, *20*, 2217. (b) Zou, Y.; Gendron, D.; Badrou-Aich, R.; Najari, A.; Tao, Y.; Leclerc, M. *Macromolecules* **2009**, *42*, 2891. (c) Yu, C.-Y.; Chen, C.-P.; Chan, S.-H.; Hwang, G.-W.; Ting, C. *Chem. Mater.* **2009**, *21*, 3262.
(126) (a) Tamayo, A. B.; Tantiwiwat, M.; Walker, B.; Nguyen, T.-Q. *J. Phys. Chem. C* **2008**, *112*, 15543. (b) Peet, J.; Tamayo, A. B.; Dang, X. D.; Seo, J. H.; Nguyen, T. Q. *Appl. Phys. Lett.* **2008**, *93*, 163306. (c) Tamayo, A. B.; Dang, X.-D.; Walker, B.; Seo, J.; Kent, T.; Nguyen, T.-Q. *Appl. Phys. Lett.* **2009**, *94*, 103301. (d) Walker, B.; Tamayo, A. B.; Dang, X.-D.; Zalar, P.; Seo, J. H.; Garcia, A.; Tantiwiwat, M.; Nguyen, T.-Q. *Adv. Funct. Mater.* **2009**, *19*, 3063.
(127) Wienk, M. M.; Turbiez, M.; Gilot, J.; Janssen, R. A. *J. Adv. Mater.* **2008**, *20*, 2556.
(128) Gadisa, A.; Mammo, W.; Andersson, L. M.; Admassie, S.; Zhang, F.; Andersson, M. R.; Inganas, O. *Adv. Funct. Mater.* **2007**, *17*, 3836.
(129) Sun, M.; Wang, L.; Xia, Y.; Du, B.; Liu, R.; Cao, Y. *Acta Polym. Sin.* **2007**, 952–958.
(130) Wang, E.; Hou, L.; Wang, Z.; Hellström, S.; Zhang, F.; Inganäs, O.; Andersson, M. R. *Adv. Mater.* **2010**, *22*, 5240–5244.
(131) Blouin, N.; Michaud, A.; Gendron, D.; Wakim, S.; Blair, E.; Neagu-Plesu, R.; Belletete, M.; Durocher, G.; Tao, Y.; Leclerc, M. *J. Am. Chem. Soc.* **2008**, *130*, 732.
(132) Park, S. H.; Roy, A.; Beaupre, S.; Cho, S.; Coates, N.; Moon, J. S.; Moses, D.; Leclerc, M.; Lee, K.; H., A. J. *Nat. Photonics* **2009**, *3*, 297.
(133) Hayakawa, A.; Yoshikawa, O.; Fujieda, T.; Uehara, K.; Yoshikawa, S. *Appl. Phys. Lett.* **2007**, *90*, 163517.
(134) Hoven, C. V.; Dang, X.-D.; Coffin, R. C.; Peet, J.; Nguyen, T.-Q.; Bazan, G. C. *Adv. Mater.* **2010**, *22*, E63.
(135) Li, Z.; Ding, J.; Song, N.; Lu, J.; Tao, Y. *J. Am. Chem. Soc.* **2010**, *132* (38), 13160.
(136) Zhou, H.; Yang, L.; Price, S. C.; Knight, K. J.; You, W. *Angew. Chem., Int. Ed.* **2010**, *49*(43), 7992.
(137) (a) Hou, J. H.; Huo, L. J.; He, C.; Yang, C. H.; Li, Y. F. *Macromolecules* **2006**, *39*, 594. (b) Hou, J. H.; Tan, Z. A.; Yan, Y.; He, Y. J.; Yang, Y. F.; Li, Y. F. *J. Am. Chem. Soc.* **2006**, *128*, 4911. (c) Li, Y. F.; Zou, Y. P. *Adv. Mater.* **2008**, *20*, 2952. (d) Zou, Y. P.; Wu, W. P.; Sang, G. Y.; Yang, Y.; Liu, Y. Q.; Li, Y. F. *Macromolecules* **2007**, *40*, 7231. (d) Zhou, E. J.; Tan, Z.; Yang, Y.; Hou, L. J.; Zou, Y. P.; Yang, C. H.; Li, Y. F. *Macromolecules* **2007**, *40*, 1831. (e) Park, J. W.; Lee, D. H.; Chung, D. S.; Kang, D. M.; Kim, Y. H.; Park, C. E.; Kwon, S. K. *Macromolecules* **2010**, *43*, 2118. (f) Chang, Y. T.; Hsu, S. L.; Su, M. H.; Wei, K. H. *Adv. Funct. Mater.* **2007**, *17*, 3326. (g) Chang, Y. T.; Hsu, S. L.; Chen, G. Y.; Su, M. H.; Singh, T. A.; Diau, E. W. G.; Wei, K. H. *Adv. Funct. Mater.* **2008**, *18*, 2356. (h) Chang, Y. T.; Hsu, S. L.; Su, M. H.; Wei, K. H. *Adv. Mater.* **2009**, *21*, 2093. (i) Huo, L.; Hou, J.; Zhang, S.; Chen, H. Y.; Yang, Y. *Angew Chem., Int. Ed.* **2010**, *49*, 1500.
(138) Yu, C. Y.; Ko, B. T.; Ting, C.; Chen, C. P. *Sol. Energy Mater. Sol. Cells* **2009**, *93*, 613.
(139) Tsai, J.; Lee, W.; Chen, W.; Yu, C.; Hwang, G.; Ting, C. *Chem. Mater.* **2010**, *22*, 3290.
(140) (a) Marder, S. R.; Cheng, L.-T.; Tiemann, B. G.; Friedli, A. C.; Blanchard-Desce, M.; Perry, J. W.; Skindhøj, J. *Science* **1994**, *263*, 511. (b) Liu, S.; Haller, M. A.; Ma, H.; Dalton, L. R.; Jang, S.-H.; Jen, A. K.-Y. *Adv. Mater.* **2003**, *15*, 603.
(141) (a) Giacalone, F.; Martin, N. *Adv. Mater.* **2010**, *22*, 4220. (b) Wuerthner, F.; Meerholz, K. *Chem.*−*Eur. J.* **2010**, *16*, 9366. (c) Inganaes, O.; Zhang, F.; Tvingstedt, K.; Andersson, L.; Hellstroem, S.; Andersson, M. R. *Adv. Mater.* **2010**, *22*, E100–E116.
(142) Shoaee, S.; Clarke, T. M.; Huang, C.; Barlow, S.; Marder, S. R.; Heeney, M.; McCulloch, I.; Durrant, J. R. *J. Am. Chem. Soc.* **2010**, *132* (37), 12919.
(143) Anthony, J. E.; Facchetti, A.; Heeney, M.; Marder, S. R.; Zhan, X. *Adv. Mater.* **2010**, *22*, 3876.
(144) Granstrom, M.; Petritsch, K.; Arias, A. C.; Lux, A.; Andersson, M. R.; Friend, R. H. *Nature* **1998**, *395*, 257.
(145) (a) Andersson, M. R.; Selse, D.; Berggren, M.; Jaervinen, H.; Hjertberg, T.; Inganas, O.; Wennerstroem, O.; Oesterholm, J. E. *Macromolecules* **1994**, *27*, 6503. (b) Pei, Q.; Jarvinen, H.; Osterholm, J. E.; Inganas, O.; Laakso, J. *Macromolecules* **1992**, *25*, 4297. (c) Johansson, T.; Mammo, W.; Svensson, M.; Andersson, M. R.; Inganas, O. *J. Mater. Chem.* **2003**, *13*, 1316. (d) Gadisa, A.; Svensson, M.; Andersson, M. R.; Inganas, O. *Appl. Phys. Lett.* **2004**, *84*, 1609. (e) deLeeuw, D. M.; Simenon, M. M. J.; Brown, A. R.; Einerhand, R. E. F. *Synth. Met.* **1997**, *87*, 53. (f) Aasmundtveit, K. E.; Samuelsen, E. J.; Mammo, W.; Svensson, M.; Andersson, M. R.; Pettersson, L. A. A.; Inganas, O. *Macromolecules* **2000**, *33*, 5481. (g) Andersson, M. R.; Berggren, M.; Inganas, O.; Gustafsson, G.; Gustafssoncarlberg, J. C.; Selse, D.; Hjertberg, T.; Wennerstrom, O. *Macromolecules* **1995**, *28*, 7525. (h) Theander, M.; Inganas, O.; Mammo, W.; Olinga, T.; Svensson, M.; Andersson, M. R. *J. Phys. Chem. B* **1999**, *103*, 7771.
(146) Holcombe, T. W.; Woo, C. H.; Kavulak, D. F.J.; Thompson, B. C.; Frechet, J. M. J. *J. Am. Chem. Soc.* **2009**, *131*, 14160.
(147) (a) Kietzke, T; Horhold, H; Neher, D. *Chem. Mater.* **2005**, *17*, 6532. (b) Alam, M. M.; Jenekhe, S. A. *Chem. Mater.* **2004**, *16*, 4647. (c) Jenekhe, S. A.; Yi, S. *Appl. Phys. Lett.* **2000**, *77*, 2635.
(148) Sang, G.; Zou, Y.; Huang, Y.; Zhao, G.; Yang, Y.; Li, Y. *Appl. Phys. Lett.* **2009**, *94*, 193302.
(149) Tan, Z. A.; Zhou, E. J.; Zhan, X. W.; Wang, X.; Li, Y. F.; Barlow, S.; Marder, S. R. *Appl. Phys. Lett.* **2008**, *93*, 073309.
(150) Mikroyannidis, J. A.; Stylianakis, M. M.; Sharma, G. D.; Balraju, P.; Roy, M. S. *J. Phys. Chem. C* **2009**, *113*, 7904.
(151) Kim, J.; Lee, S.; Toney, M.; Chen, Z.; Facchetti, A.; Kim, Y. S.; Loo, Y.-L. *Chem. Mater.* **2010**, *22*, 0.
(152) Alam, M. M.; Jenekhe, S. A. *Chem. Mater.* **2004**, *16*, 4647.
(153) King, S.; Sommer, M.; Huettner, S.; Thelakkat, M.; Haque, S. A. *J. Mater. Chem.* **2009**, *19*, 5436.
(154) Zhang, Q.; Cirpan, A.; Russell, T. P.; Emrick, T. *Macromolecules* **2009**, *42*, 1079.
(155) Sang, G.; Zou, Y.; Huang, Y.; Zhao, G.; Yang, Y.; Li, Y. *Appl. Phys. Lett.* **2009**, *94*, 193302.